

Department of Applied Physics

# Collective excitations in ultracold Fermi gases

---

Anna Korolyuk

# Collective excitations in ultracold Fermi gases

**Anna Korolyuk**

Doctoral dissertation for the degree of Doctor of Science in  
Technology to be defended, with the permission of the Aalto  
University School of Science (Espoo, Finland), at a public  
examination held at the lecture hall E of the school on 9 May 2014  
at 12.

**Aalto University**  
**School of Science**  
**Department of Applied Physics**

**Supervising professor**

Prof. Päivi Törmä

**Thesis advisors**

Prof. Päivi Törmä

Dr. Jami Kinnunen

**Preliminary examiners**

Prof. Esa Räsänen, Tampere University of Technology, Finland

Prof. Robert van Leeuwen, University of Jyväskylä, Finland

**Opponent**

Prof. Georg Bruun, Aarhus University, Denmark

Aalto University publication series

**DOCTORAL DISSERTATIONS 45/2014**

© Anna Korolyuk

ISBN 978-952-60-5635-7

ISBN 978-952-60-5636-4 (pdf)

ISSN-L 1799-4934

ISSN 1799-4934 (printed)

ISSN 1799-4942 (pdf)

<http://urn.fi/URN:ISBN:978-952-60-5636-4>

Unigrafia Oy

Helsinki 2014

Finland

Publication orders (printed book):

[anna.korolyuk@gmail.com](mailto:anna.korolyuk@gmail.com)

**Author**

Anna Korolyuk

**Name of the doctoral dissertation**

Collective excitations in ultracold Fermi gases

**Publisher** School of Science

**Unit** Department of Applied Physics

**Series** Aalto University publication series DOCTORAL DISSERTATIONS 45/2014

**Field of research** Ultracold Fermi gases

**Manuscript submitted** 6 April 2014

**Date of the defence** 9 May 2014

**Permission to publish granted (date)** 24 March 2014

**Language** English

**Monograph**

**Article dissertation (summary + original articles)**

**Abstract**

Ultracold gases are of great interest in modern physics. The main reason is that in the systems of ultracold gases the parameters can be easily tuned, thus they can be used as a testing ground for various quantum many-body theories. Interesting macroscopic quantum effects have been observed in the ultracold gas systems, for instance Bose-Einstein condensation. In this thesis, theoretical knowledge of ultracold gases is extended. A summary of the methods used in this thesis is given, including a detailed description of the density response theory and the time-evolving block decimation (TEBD) algorithm. Collective excitations of an ultracold gas in a three-dimensional (3D) spherically symmetric trap are studied in detail in publications II and III. As a result, several collective modes are discovered such as a low energy Higgs-type mode, a second sound-like mode, and a strong mode resembling the Leggett mode. Using the TEBD algorithm, physics of a polaron in a one-dimensional (1D) lattice, and the Fulde-Ferrell-Larkin-Ovchinnikov (FFLO) state in 1D are studied in publications IV and I, respectively. In publication I a method to detect the FFLO phase is suggested, namely by the observation of the change in the double occupancy after a lattice depth modulation. Publication IV compares a variational ansatz and the TEBD simulations and finds an excellent agreement, indicating that the variational ansatz can be used to describe the system for a certain range of interactions.

**Keywords** Fermi gas, TEBD, FFLO, cold gases, superfluidity, collision dynamics, collective excitations

**ISBN (printed)** 978-952-60-5635-7

**ISBN (pdf)** 978-952-60-5636-4

**ISSN-L** 1799-4934

**ISSN (printed)** 1799-4934

**ISSN (pdf)** 1799-4942

**Location of publisher** Helsinki

**Location of printing** Helsinki

**Year** 2014

**Pages** 109

**urn** <http://urn.fi/URN:ISBN:978-952-60-5636-4>



**Tekijä**

Anna Korolyuk

**Väitöskirjan nimi**

Collective excitations in ultracold Fermi gases

**Julkaisija** Perustieteiden korkeakoulu**Yksikkö** Department of Applied Physics**Sarja** Aalto University publication series DOCTORAL DISSERTATIONS 45/2014**Tutkimusala** Ultracold Fermi gases**Käsitteilyajon pvm** 06.04.2014**Väitöspäivä** 09.05.2014**Julkaisuluvan myöntämispäivä** 24.03.2014**Kieli** Englanti **Monografia** **Yhdistelmäväitöskirja (yhteenvedo-osa + erillisartikkelit)****Tiivistelmä**

Ultrakylmät atomikaasut ovat keskeisiä modernin fysiikan tutkimuskohteita. Ensisijainen syy tähän on, että ultrakylmien kaasujen parametreja on helppo säätää, minkä vuoksi niitä voidaan käyttää erilaisten kvanttimekaniikan monihiukkasteorioiden testaamiseen. Mielenkiintoisia makroskooppisia kvanttiefektejä on havaittu ultrakylmissä atomikaasuissa, esimerkiksi Bose-Einstein kondensaatio.

Tässä väitöskirjassa on tutkittu ultrakylmiä atomikaasuja teoreettisesti. Kirjassa esitetään tiivistelmä työssä käytetyistä menetelmistä, mukaan lukien yksityiskohtainen kuvaus tiheysvastateoriasta ja niin sanotusta TEBD (time-evolving block decimation) algoritmista. Kollektiivisiä eksitaatioita kolmiulotteisissa pallosymmetrisissä atomikaasuissa on tutkittu julkaisuissa II ja III. Tuloksena löydettiin useita kollektiivisiä moodeja, kuten alhaisen energian Higgs-tyyppinen moodi, toinen äänimoodi, sekä voimakas Leggett-tyyppinen moodi. Julkaisuissa I ja IV tutkittiin TEBD-algoritmia käyttäen polaronin fysiikkaa sekä Fulde-Ferrell-Larkin-Ovchinnikov (FFLO) tilaa yksiulotteisessa hilassa. Julkaisussa I kehitettiin menetelmä, jolla FFLO-tila voitaisiin havaita kokeellisesti tarkastelemalla muutosta kaksoismiehityksessä hilan syvyyttä moduloitaessa. Julkaisussa IV verrattiin variaatiolauseketta ja TEBD-simulaatioita. Tulokset olivat hyvin samanlaiset, mikä osoittaa että variaatiolauseketta voidaan käyttää järjestelmän kuvaamiseen tietyssä vuorovaikutusalueessa.

**Avainsanat** Fermikaasut, TEBD, FFLO, kylmät kaasut, suprajooksevuus, törmäysdynamikka, kollektiiviset eksitaatiot

**ISBN (painettu)** 978-952-60-5635-7**ISBN (pdf)** 978-952-60-5636-4**ISSN-L** 1799-4934**ISSN (painettu)** 1799-4934**ISSN (pdf)** 1799-4942**Julkaisupaikka** Helsinki**Painopaikka** Helsinki**Vuosi** 2014**Sivumäärä** 109**urn** <http://urn.fi/URN:ISBN:978-952-60-5636-4>



# Preface

The work presented here is based on the research I have carried out during the years 2008-2014 at Aalto University School of Science, Finland. I would have never succeed with it without the enormous help from people who surrounded me.

First of all, I want to thank to my supervising professor Prof. Päivi Törmä. Her extremely high level of professionalism together with freedom she gives to researchers formed me as a professional. Also I want to thank to my supervisor Dr. Jami Kinnunen - without his patient answers to my questions this thesis would not have be completed. Dr. Francesco Massel, Dr. Jani-Petri Martikainen and Dr. Dong-Hee Kim guided me in the world of ultracold gases as well as Dr. Timo Koponen, Dr. Mikko Leskinen and Dr. Jussi Kajala. I want to thank Mr. Elmer Doggen and Miss Anne-Maria Visuri for fruitful discussions as well as Mr. Miikka Heikkinen and Dr. Antti-Pekka Eskelinen. Sincere thanks go also to Dr. Reza Bakhtiari, Dr. Tommi Hakala, Dr. Marcus Rinkiö, Dr. Tuomas Lahtinen, Mrs. Laura Äkäslömpö, Mr. Olli Nummi and Dr. Anton Kuzyk. Finally, scientific work would not have been easy without the help of Mr. Mikael Henny and Dr. Marika Linja.

The pre-examinors of this thesis, Prof. Robert van Leeuwen and Associate Prof. Esa Räsänen gave valuable corrections and suggestions concerning my thesis. I am grateful for them for the careful reading of my thesis and the insightful comments that helped me to improve it.

My acknowledgements would not be complete without mentioning my Ukrainian teachers and tutors. I would like to thank my high school teacher Raisa Kuzyk from Lviv Physics and Mathematics Lyceum for teaching us about the importance of education. I would like to thank Prof. Stanislav Vilchynskyy from Kyiv national Taras Shevchenko university for supporting me and other physics students when we just started our scientific careers. I would like to thank to Dr. Vitalij Shadura from the Center of Young Scientists at Bogolyubov Institute

for Theoretical Physics for creating learning environment for young scientists. And I would like to thank to Prof. Valerij Gusynin for being the supervisor of my Master's thesis.

During my PhD studies I was lucky to gain experience outside of science. I want to thank Prof. Yrjö Neuvo for the Bit Bang course and directing me towards thinking about practical applications of research. I want to thank Juha Makkonen, Antti Virolainen, and Niklas Begley for giving me the opportunity of working for Sharetribe/Kassi and learning about a start-up environment from inside. Also I want to thank Maiju Airosmäa and Anne Badan for our work together at Aalto Social Impact.

And finally I would like to thank people who were not contributing directly to my scientific research, but who kept me motivated during such a big project and without whom this work no doubt would not have been finished. First of all I want to thank Natalia for encouraging me to have goals in life and to move towards them. Also I want to thank Alex for supporting me when everything looked hopeless. I want to thank my Finnish friends, Antti and Annina for a warm welcome to Finland, Eugene and Iryna for creating a small Ukraine here, and Eugene and Jelizaveta for rising my interest not only in technology, but also in humanistic sciences. I want to thank my dearest Vivian for a lot of support during the toughest last year of studies and Meri for being a friend. I want to thank Aleksii for showing me the heart of the Finnish country and that I feel as at home here. And finally I want to thank my family, father Pavlo, mother Olexandra and sister Maria for love and unconditional support during the last 15 years I was studying physics.

Helsinki, April 5, 2014,

# Contents

<b>Preface</b>	<b>1</b>
<b>Contents</b>	<b>3</b>
<b>List of Publications</b>	<b>5</b>
<b>Author's Contribution</b>	<b>7</b>
<b>1. Introduction</b>	<b>9</b>
<b>2. Theoretical descriptions of ultracold Fermi gases</b>	<b>13</b>
2.1 Hamiltonian for the ultracold gas . . . . .	13
2.1.1 Scattering length, Feshbach resonance, unitarity . . . . .	13
2.1.2 The Hamiltonian . . . . .	15
2.1.3 Mean field and Bogolyubov-deGennes Equations . . . . .	16
2.1.4 Optical lattices . . . . .	18
2.1.5 Hamiltonian in a lattice . . . . .	20
2.2 BCS theory and superfluidity . . . . .	21
2.2.1 Cooper pairs . . . . .	22
2.2.2 Imbalanced gas . . . . .	24
2.2.3 The FFLO state and exotic superfluidity . . . . .	25
<b>3. Density response</b>	<b>27</b>
3.1 General theory of the response function . . . . .	27
3.2 Collective frequencies in the response function . . . . .	29
3.3 Linear density response . . . . .	31
3.4 Introducing the angular momentum . . . . .	34
3.5 Bogolyubov-deGennes equations and density response . . . . .	36
3.6 Key results . . . . .	38
<b>4. TEBD (Time-Evolving Block Decimation) method</b>	<b>43</b>

4.1	DMRG (Density Matrix Renormalization Group) method . . . . .	43
4.2	TEBD: Schmidt decomposition . . . . .	44
4.3	TEBD algorithm . . . . .	48
4.3.1	Hamiltonian $\hat{H}_i$ for one lattice site . . . . .	48
4.3.2	Hamiltonian $\hat{H}_{i,i+1}$ for two adjacent lattice sites . . . . .	50
4.3.3	Time-evolution . . . . .	51
4.3.4	Ground state . . . . .	52
4.4	Key results . . . . .	53
<b>5.</b>	<b>Conclusions</b>	<b>55</b>
	<b>Bibliography</b>	<b>57</b>
	<b>Publications</b>	<b>65</b>

# List of Publications

This thesis consists of an overview and of the following publications which are referred to in the text by their Roman numerals.

**I** A. Korolyuk, F. Massel, and P. Törmä. Probing the Fulde-Ferrell-Larkin-Ovchinnikov Phase by Double Occupancy Modulation Spectroscopy. *Physical Review Letters*, 104, 236402, 2010.

**II** A. Korolyuk, J. J. Kinnunen, and P. Törmä. Density response of a trapped Fermi gas: A crossover from the pair vibration mode to the Goldstone mode. *Physical Review A*, 84, 033623, 2011.

**III** A. Korolyuk, J. J. Kinnunen, and P. Törmä. Collective excitations of a trapped Fermi gas at finite temperature. *Physical Review A*, 89, 013602, 2014.

**IV** E. V. H. Doggen, A. Korolyuk, P. Törmä and J. J. Kinnunen. One-dimensional Fermi polaron in a combined harmonic and periodic potential. *Submitted to Physical Review A and to the arxiv preprint server*  
<http://arxiv.org/abs/1401.6353>, 2014.



# Author's Contribution

## **Publication I: “Probing the Fulde-Ferrell-Larkin-Ovchinnikov Phase by Double Occupancy Modulation Spectroscopy”**

The author carried out numerical calculations for this paper and greater part of analysis of the result. The author participated in writing the publication.

## **Publication II: “Density response of a trapped Fermi gas: A crossover from the pair vibration mode to the Goldstone mode”**

The author carried out analytical and numerical calculations and analysis of the obtained data for this paper. The author actively participated in writing the publication.

## **Publication III: “Collective excitations of a trapped Fermi gas at finite temperature”**

The author suggested the use of the singular value decomposition in the simulations and carried out the numerical calculations and data analysis. The author wrote a major part of the publication.

## **Publication IV: “One-dimensional Fermi polaron in a combined harmonic and periodic potential”**

The author carried out part of the numerical calculations for this paper and participated in writing the publication.



# 1. Introduction

## Ultracold gases as a testbed for quantum physics

Ultracold gases are known to be one of the most beautiful laboratories for investigating quantum systems. Variety of experiments can be performed and diverse theories can be tested. Some of these experiments are essentially unique and cannot be conducted in other systems. One of the reasons for this uniqueness is that many key parameters for ultracold gas can be varied across a very wide range; for example the interaction between the particles can be both attractive and repulsive and of any magnitude. This tunability is the key factor why with ultracold gases many important achievements have been possible such as Bose-Einstein condensation, Fermi condensates, and associated vortex experiments.

With ultracold gases, it is possible to observe macroscopic quantum phenomena or macroscopic quantum coherence [1–5]. The general definition of a macroscopic quantum effect is a quantum phenomenon that involves a macroscopic number of particles, or the wave function has a macroscopic size. The most known ones are superfluidity in superfluid helium, superconductivity in superconductors, and the coherence of laser light.

The most famous example of a macroscopic quantum phenomenon in ultracold gases is Bose-Einstein condensation (BEC). It was initially predicted by Bose in 1924 [6] and Einstein in 1925 [7], but achieved in a clear form only in 1995 [8, 9]. Bose-Einstein condensation also plays a role in superfluidity of Helium, but the condensate fraction is small. During the experiment [8] Rubidium atoms were cooled down to 170 nK. At such a low temperature the majority of bosons are in the lowest energy quantum state, and this is called condensation. The temperature must be lower than critical temperature  $T_c$  of the condensation, which depends on the density of the gas  $n$ :  $T_c \sim n^{\frac{2}{3}}$  in three-dimensional

(3D) case. One can observe BEC in Bose gases or in Fermi gases when bosonic pairs of two Fermi atoms are formed. Recently a BEC was observed experimentally for photons [10], magnons [11] and exciton polaritons [12].

The breakthrough experiments that achieved Bose-Einstein condensation were performed in 1995 with rubidium atoms [8] and with sodium atoms [9]. Later, in 2003, condensates consisting of Fermi atoms was created too [13–15]. From all these experiments a new branch of science was started - the research of ultracold gases, both fermionic and bosonic.

Cooling atoms to such low temperatures can be done using two main techniques, namely laser cooling and evaporative cooling [16–21]. In laser cooling, as the atoms are moving towards the laser beam, their resonant frequency is slightly changed due to the Doppler effect. The frequency of the laser light is now such that atoms in the laser beam first absorb photons and then they emit photons with a slightly different energy. Only atoms moving towards (not from) the laser beam absorb photons, so atoms are lowering their momenta and thus cooled. This method allows atoms to cool down to  $10^{-6}$  K, which is low enough, but still 100 times too hot for creating BEC. After the atoms are cooled with the laser beams, evaporative cooling can be applied. The name of the process reflects its similarity to the process of for instance evaporation of coffee in a cup. The atoms are trapped by magnetic or light field, but the trap is adjusted in such a way that the fastest atoms manage to leave the trap, thus taking energy away and cooling down the gas.

Returning to the tunability of ultracold gases, experimentally it is implemented by controlling external electromagnetic fields. For instance, interaction in a trapped gas can be controlled via the Feshbach resonance [22–27]. Spin-dependent interatomic interaction depends on the external magnetic field, so by tuning it one can influence both the magnitude and the sign of the interaction. For a gas in a lattice, additionally the hopping and coupling parameters of the Hubbard Hamiltonian depend on the intensity and the frequency of the controlling laser beams. An additional level of freedom is that ultracold gases can be realized in different geometrical configurations. For instance, they can exist in different dimensions (1D, 2D, 3D) and for various lattice and trap geometries [28–32].

So far there are not many practical applications for ultracold atomic gases, although quite a lot of research is on the way. The most famous perspectives are quantum simulators (physical systems which can simulate the behavior of other quantum systems) [33–36] and quantum computers (quantum systems which perform operations on data). The other promising engineering applica-

tions are more precise atomic clocks [37] and gravitational sensors [38].

With the help of collective excitations one can perform a deep analysis of the properties of a many-body quantum system. In ultracold gases the collective excitations have been studied extensively, see for example [39, 40]. Hydrodynamic models [41] describe well these collective modes in a strongly and weakly interacting limits, but in general case they are not sufficient. To complement these simple models, a more microscopic theory using random phase approximation can be applied [42–44].

Imbalanced ultracold gases, or gases with unequal number of particles in different spin states, are of a great interest too [45–47]. In one dimension, experimental results that are consistent with the exotic Fulde-Ferrell-Larkin-Ovchinnikov (FFLO) state have been reported, but direct evidence of the FFLO state is still missing [47]. Polaron, a special case of an imbalanced gas with only one atom in one of the spin states, has been experimentally investigated as well [48–50].

In this thesis the author investigates collective excitations for certain configurations of ultracold Fermi gas systems. Particularly, ultracold gases in a spherically symmetric three-dimensional (3D) trap are considered in detail (Publications II and III). Additionally, gases in one-dimensional (1D) traps are also studied (Publications I and IV). The main results the author has achieved are a suggestion of a novel method for detecting of the FFLO state, which is a state of exotic superfluidity, and detailed description of the collective excitations of the ultracold gas in a spherically symmetric 3D trap. In particular, a second sound-like mode, a Higgs-like mode and a Leggett-mode type edge mode were found.

This thesis is organized as follows. In Chapter 2, various theoretical approaches to ultracold Fermi gases are discussed. First, the Hamiltonian is discussed, then the mean-field and Bogolyubov-de-Gennes theory, and finally exotic superfluid states such as FFLO. In Chapter 3, density response theory is discussed. This is the main method used in publications II and III. In Chapter 4, the TEBD algorithm is reviewed: it was used in publications I and IV. In Chapter 5, the key results of this thesis are summarized.



## 2. Theoretical descriptions of ultracold Fermi gases

Here an overview of some of the important theories used for the description of ultracold Fermi gases is presented. In Section 2.1, the basics are discussed such as the scattering amplitude and the scattering length, the Hamiltonians both for a trap and a lattice are introduced, and mean-field theory is outlined. In Section 2.2, the general theory of Cooper pairs is used as a framework for discussing pairing in ultracold gases, especially paying attention to exotic superfluid states such as the Fulde-Ferrell-Larkin-Ovchinnikov (FFLO) state.

### 2.1 Hamiltonian for the ultracold gas

#### 2.1.1 Scattering length, Feshbach resonance, unitarity

To model an ultracold gas system, two-body interactions must be introduced first. For ultracold gases, as they are dilute and at low temperatures, the details of the two-body interactions are not important. Instead, the atom-atom interaction can be described by utilizing the two-body scattering amplitude. The simplest scattering amplitude which describes ultracold gases well is the s-wave amplitude (spherically symmetric scattering is assumed) [32, 41]:

$$F(k) = -\frac{1}{a^{-1} - \frac{1}{2}k^2 R^* + ik}. \quad (2.1)$$

Here  $a$  is the scattering length,  $R^*$  is the effective range of the interaction, and  $k$  is the momentum involved in the scattering. Usually for ultracold gases  $kR^* \ll 1$ , so

$$F(k) = -\frac{1}{a^{-1} + ik}. \quad (2.2)$$

Such a scattering amplitude corresponds to the pseudopotential:

$$V_{eff}(r) = g\delta(\mathbf{r})\frac{\partial}{\partial r}r, \quad (2.3)$$

where the coupling constant  $g$  is defined via the scattering length  $a$  as  $g = \frac{4\pi\hbar^2 a}{m}$ . This potential is called “the contact potential” and is often used for ultracold gases. However, in practice the potential  $V_{eff}(r) = g\delta(\mathbf{r})$  is used, which is simpler but together with introducing a cut-off is equivalent to the potential of Equation 2.3.

The scattering length  $a$  [51–53] can have any value, positive and negative, including infinity. The scattering length  $a$  is infinite in the so-called unitarity limit, which in ultracold gases exists due to the Feshbach resonance. Consider two interacting atoms with van der Waals type interaction.

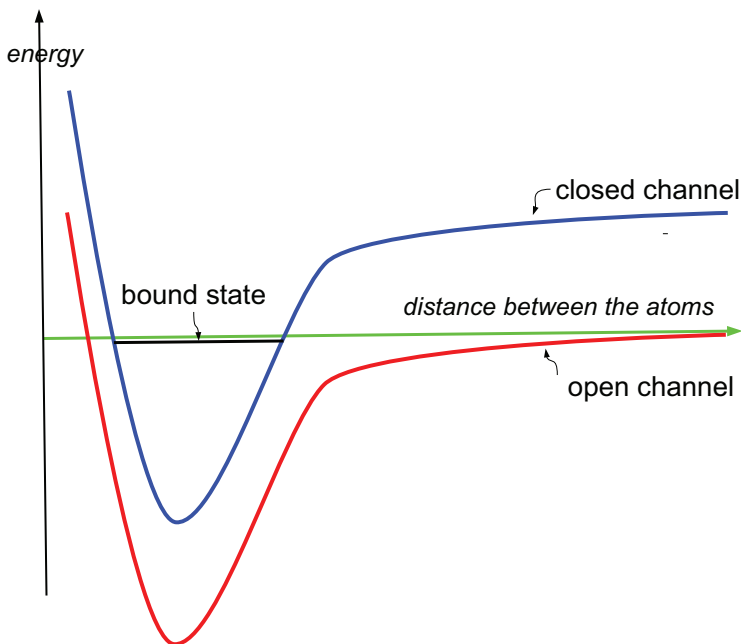


**Figure 2.1.** Schematic description of a Feshbach resonance. The picture shows the dependence of the potential energy (van der Waals type) on the distance between the two atoms. The blue line marks the closed channel, the red line shows the open channel. When energies of the open scattering state and bound state coincide (green line), virtual transitions between those two states are allowed: this is called the Feshbach resonance.

Figure 2.1 shows a schematic picture of the two-body potential. The main point is that regardless of the exact features of the potential, two scattering particles in two different spin-configurations will follow two potentials of the same shape, which are shifted relative to each other due to an external magnetic field (Zeeman effect). In Figure 2.1 energy potentials for two particles with

different spin-configurations are shown by blue and red colors. The two-body potential has bound states and open scattering states, which are significantly shifted from each other. But it may happen that two atomic configurations with different spins, one in open channel, the other corresponding to some bound state in closed channel, have the same (or very closely to the same) energy. In that case, the two levels are in resonance and the effective interaction between the two atoms increases to infinity. This is called the Feshbach resonance and corresponds to the unitarity limit. In this case, scattering amplitude for the long wavelength ( $k \rightarrow 0$ ) limit is approaching infinity  $F(0) \rightarrow \infty$  and effectively one can consider the gas as having infinite two-body interaction. The unitarity is a transition point between the Bardeen-Cooper-Schrieffer (BCS) side (attractive interaction,  $a < 0$ , the atoms form Cooper pairs) and the BEC side (repulsive interaction,  $a > 0$ , the atoms form bound dimers). Formally, this transition happens when the scattering length increases from  $a = +0$  to  $a = +\infty$ , jumps from  $a = +\infty$  to  $a = -\infty$  (unitarity), and then decreases from  $a = -\infty$  to  $a = -0$ .

The scattering length changes as a function of the external magnetic field  $B$  in the following way [41]:

$$a(B) = a_{bg} \left( 1 - \frac{\Delta B}{B - B_0} \right), \quad (2.4)$$

where  $a_{bg}$  is the scattering length in the absence of a Feshbach resonance,  $B_0$  is the critical magnetic field for which  $a = \infty$  (unitarity point) and  $\Delta B$  is the width of the resonance. Due to the multitude of molecular bound states, there are many resonances. However, some resonances are more relevant experimentally and easier to utilize. For example, for  $^{40}\text{K}$  a useful resonance is at  $B_0 = 202\text{G}$  [54] and for  $^6\text{Li}$  at  $B_0 = 834\text{G}$  [55]. There exists also a Feshbach resonance for  $^6\text{Li}$  at  $B_0 = 543\text{G}$  [56], but it is of different type, namely a so-called 'narrow resonance'. The difference between narrow and wide resonances is that for wide resonances the effective range  $R^*$  (mentioned in Equation 2.1) is small,  $k_F |R^*| \ll 1$ , and for narrow resonances it is large  $k_F |R^*| > 1$  [57, 58]. Thus for wide resonances,  $R^*$  is not a relevant lengthscale any more and only the scattering length  $a$  matters (and the scattering amplitude is  $F(k) = -\frac{1}{a^{-1} + ik}$ ); for a narrow resonance,  $R^*$  must also be taken into account.

### 2.1.2 The Hamiltonian

The basic Hamiltonian for fermions in an external potential (e.g. a trap as shown in Figure 2.2) is the following:

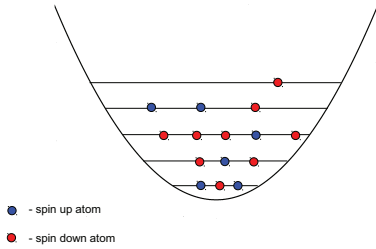


**Figure 2.2.** Ultracold atoms with different spins in a 3D trap. Blue marks atoms with spin up, red - with spin down. In a 3D trap the distance between energy levels is  $2\omega_T$ , where  $\omega_T$  is the trap frequency. For 3D traps, the levels are degenerate (for the same energy, there are multiple levels with different angular momenta). That is why a few atoms with the same spin are shown on the same level: in reality they have the same energy but different angular momenta.

$$\begin{aligned} \hat{H} = & \sum_{s=\{\uparrow, \downarrow\}} \int d\mathbf{r} \hat{\Psi}_s^\dagger(\mathbf{r}) \left( -\frac{\hbar^2 k^2}{2m_s} + V_{s,ext}(\mathbf{r}) - \mu_s \right) \hat{\Psi}_s(\mathbf{r}) \\ & + \int d\mathbf{r} d\mathbf{r}' V(\mathbf{r}-\mathbf{r}') \hat{\Psi}_\uparrow^\dagger(\mathbf{r}) \hat{\Psi}_\downarrow^\dagger(\mathbf{r}') \hat{\Psi}_\downarrow(\mathbf{r}') \hat{\Psi}_\uparrow(\mathbf{r}), \end{aligned} \quad (2.5)$$

where the field operators  $\Psi, \Psi^\dagger$  are fermionic, that is  $\{\hat{\Psi}_s^\dagger(\mathbf{r}), \hat{\Psi}_{s'}(\mathbf{r}')\} = \delta_{ss'} \delta(\mathbf{r}-\mathbf{r}')$ . The first term takes into account the kinetic energy  $-\frac{\hbar^2 k^2}{2m_s}$  ( $m_s$  is the mass of an atom with spin  $s$ ), the external (e.g. trap) potential  $V_{s,ext}(\mathbf{r})$  and the chemical potential  $\mu_s$ . The second term is a two-body interaction: the simplest potential for ultracold gas systems is a contact potential

$$V(\mathbf{r}-\mathbf{r}') = g\delta(\mathbf{r}-\mathbf{r}'). \quad (2.6)$$

Using the contact potential, the Hamiltonian of Equation 2.5 becomes

$$\begin{aligned} \hat{H} = & \sum_{s=\{\uparrow, \downarrow\}} \int d\mathbf{r} \hat{\Psi}_s^\dagger(\mathbf{r}) \left( -\frac{\hbar^2 k^2}{2m_s} + V_{s,ext}(\mathbf{r}) - \mu_s \right) \hat{\Psi}_s(\mathbf{r}) \\ & + g \int d\mathbf{r} \hat{\Psi}_\uparrow^\dagger(\mathbf{r}) \hat{\Psi}_\downarrow^\dagger(\mathbf{r}) \hat{\Psi}_\downarrow(\mathbf{r}) \hat{\Psi}_\uparrow(\mathbf{r}). \end{aligned} \quad (2.7)$$

### 2.1.3 Mean field and Bogolyubov-deGennes Equations

The Hamiltonian of Equation 2.7 can very seldom be exactly solved. Therefore mean-field theories, such as the Bogolyubov-deGennes theory, are often used. In mean-field theories, the original Hamiltonian with full two-body interactions is replaced by an effective Hamiltonian with a simplified two-body interaction term.

The Hamiltonian of Equation 2.7 contains the kinetic energy term  $K = \sum_{s=\{\uparrow, \downarrow\}} \int d\mathbf{r} \hat{\Psi}_s^\dagger(\mathbf{r})(\dots)\hat{\Psi}_s(\mathbf{r})$  and the many-body interaction  $g \int d\mathbf{r} \hat{\Psi}_\uparrow^\dagger(\mathbf{r})\hat{\Psi}_\downarrow^\dagger(\mathbf{r})\hat{\Psi}_\downarrow(\mathbf{r})\hat{\Psi}_\uparrow(\mathbf{r})$ .

The latter one can be approximated as [59]

$$\begin{aligned}
& \hat{\Psi}_\uparrow^\dagger(\mathbf{r})\hat{\Psi}_\downarrow^\dagger(\mathbf{r})\hat{\Psi}_\downarrow(\mathbf{r})\hat{\Psi}_\uparrow(\mathbf{r}) \\
& \sim \hat{\Psi}_\uparrow^\dagger(\mathbf{r})\hat{\Psi}_\downarrow^\dagger(\mathbf{r})\langle\hat{\Psi}_\downarrow(\mathbf{r})\hat{\Psi}_\uparrow(\mathbf{r})\rangle + \langle\hat{\Psi}_\uparrow^\dagger(\mathbf{r})\hat{\Psi}_\downarrow^\dagger(\mathbf{r})\rangle\hat{\Psi}_\downarrow(\mathbf{r})\hat{\Psi}_\uparrow(\mathbf{r}) \\
& + \langle\hat{\Psi}_\downarrow^\dagger(\mathbf{r})\hat{\Psi}_\uparrow^\dagger(\mathbf{r})\rangle\hat{\Psi}_\uparrow^\dagger(\mathbf{r})\hat{\Psi}_\downarrow(\mathbf{r}) + \hat{\Psi}_\uparrow^\dagger(\mathbf{r})\hat{\Psi}_\downarrow(\mathbf{r})\langle\hat{\Psi}_\uparrow^\dagger(\mathbf{r})\hat{\Psi}_\downarrow^\dagger(\mathbf{r})\rangle \quad (2.8) \\
& = \hat{\Psi}_\uparrow^\dagger(\mathbf{r})\hat{\Psi}_\downarrow^\dagger(\mathbf{r})\Delta(\mathbf{r}) + \hat{\Psi}_\downarrow(\mathbf{r})\hat{\Psi}_\uparrow(\mathbf{r})\Delta^*(\mathbf{r}) \\
& + \hat{\Psi}_\uparrow^\dagger(\mathbf{r})\hat{\Psi}_\uparrow(\mathbf{r})n_\downarrow(\mathbf{r}) + \hat{\Psi}_\downarrow^\dagger(\mathbf{r})\hat{\Psi}_\downarrow(\mathbf{r})n_\uparrow(\mathbf{r}),
\end{aligned}$$

where  $\langle\dots\rangle$  means quantum average. Here the gap  $\Delta(\mathbf{r})$  and the densities  $n_\uparrow(\mathbf{r}), n_\downarrow(\mathbf{r})$  (which are constructed from the wave function itself) are effectively playing the role of an external field. The Hamiltonian of Equation 2.7 now transforms into a mean-field Hamiltonian:

$$\begin{aligned}
\hat{H}_{MF} = K + \int d\mathbf{r} \left[ \Delta(\mathbf{r})\hat{\Psi}_\uparrow^\dagger(\mathbf{r})\hat{\Psi}_\downarrow^\dagger(\mathbf{r}) + \Delta^*(\mathbf{r})\hat{\Psi}_\downarrow(\mathbf{r})\hat{\Psi}_\uparrow(\mathbf{r}) \right. \\
\left. + gn_\downarrow(\mathbf{r})\hat{\Psi}_\uparrow^\dagger(\mathbf{r})\hat{\Psi}_\uparrow(\mathbf{r}) + gn_\uparrow(\mathbf{r})\hat{\Psi}_\downarrow^\dagger(\mathbf{r})\hat{\Psi}_\downarrow(\mathbf{r}) \right], \quad (2.9)
\end{aligned}$$

where the pairing field is

$$\Delta(\mathbf{r}) = g\langle\hat{\Psi}_\downarrow(\mathbf{r})\hat{\Psi}_\uparrow(\mathbf{r})\rangle \quad (2.10)$$

and the densities are

$$n_s(\mathbf{r}) = \langle\hat{\Psi}_s^\dagger(\mathbf{r})\hat{\Psi}_s(\mathbf{r})\rangle \quad (2.11)$$

for  $s = \{\uparrow, \downarrow\}$ .

As any quadratic Hamiltonian, the Hamiltonian of Equation 2.9 can be diagonalized:

$$\hat{H}_{MF} = \sum_{n,\alpha} E_n \gamma_{n\alpha}^\dagger \gamma_{n\alpha}, \quad (2.12)$$

where the quasiparticle operators  $\gamma_{n\alpha}^\dagger, \gamma_{n\alpha}$  correspond to eigenvectors of the Hamiltonian 2.9,  $n, \alpha$  are indices numbering them, and  $\alpha = \{1, 2\}$  or  $\alpha = \{\uparrow, \downarrow\}$  is a pseudospin.

Such a Hamiltonian has a solution of the form

$$\Psi_\uparrow = \sum_n u_n(\mathbf{r})\gamma_{n\uparrow} + v_n^*(\mathbf{r})\gamma_{n\downarrow}^\dagger \quad (2.13)$$

$$\Psi_{\downarrow} = \sum_n u_n(\mathbf{r}) \gamma_{n\downarrow} - v_n^*(\mathbf{r}) \gamma_{n\uparrow}^{\dagger}, \quad (2.14)$$

where the functions  $u_n(\mathbf{r})$  and  $v_n(\mathbf{r})$  are the solutions of the following matrix equation:

$$\begin{pmatrix} K + gn_{\uparrow}(\mathbf{r}) & \Delta(\mathbf{r}) \\ \Delta(\mathbf{r}) & -K - gn_{\downarrow}(\mathbf{r}) \end{pmatrix} \begin{pmatrix} u_n(\mathbf{r}) \\ v_n(\mathbf{r}) \end{pmatrix} = E_n \begin{pmatrix} u_n(\mathbf{r}) \\ v_n(\mathbf{r}) \end{pmatrix}, \quad (2.15)$$

and  $\{\gamma_{n\alpha}^{\dagger}, \gamma_{n'\alpha'}\} = \delta_{nn'}\delta_{\alpha\alpha'}$  are the creation and annihilation quasiparticle operators. Equations 2.15 are called the Bogolyubov-de-Gennes (BdG) equations.

To solve the BdG equations, it is necessary to combine Equation 2.15 with two equations following from self-consistency requirements:

$$\Delta(\mathbf{r}) = -\sum_n 2u_n(\mathbf{r})v_n(\mathbf{r}) \quad (2.16)$$

and

$$n_{\uparrow}(\mathbf{r}) = n_{\downarrow}(\mathbf{r}) = \sum_n |u_n(\mathbf{r})|^2 + |v_n(\mathbf{r})|^2. \quad (2.17)$$

Iteratively, solutions  $u_n(\mathbf{r})$  and  $v_n(\mathbf{r})$  of Equation 2.15 are substituted into Equations 2.16 and 2.17. Then new  $\Delta(\mathbf{r})$  and  $n_{\uparrow}(\mathbf{r}), n_{\downarrow}(\mathbf{r})$  are calculated again and substituted back into Equation 2.15. This is done until convergence is reached. The method is typically very robust for a balanced gas.

The Bogolyubov-de-Gennes mean field theory was used in publications II and III, exactly in the way described above (an iteration process). The resulting functions  $u_n(\mathbf{r})$  and  $v_n(\mathbf{r})$  are interesting to know, but in our case the purpose was to use them not directly but to construct from them a Green's function and to use that to calculate the density response.

### 2.1.4 Optical lattices

Optical lattices are one of the most prominent systems for studying ultracold gases in different quantum states. Compared to a trap, a lattice allows more precise tunability, a possibility to reach the high-density limit (high filling fractions) and a direct analogy to solid state systems. In the lattice, it is possible to both simulate already existing quantum systems (e.g. high-temperature superconductivity) and to create novel quantum systems, such as exotic superfluidity.

Optical lattices are created as following. In the electric field  $\mathbf{E}(\mathbf{r})$ , an atom with a dipole momentum  $\alpha$  experiences a dipole force  $\mathbf{F} = \frac{1}{2}\alpha\nabla(E^2(r))$ , where  $E(r)$  is the absolute value of the vector  $\mathbf{E}(\mathbf{r})$  and  $\nabla$  is the gradient  $\left(\frac{\partial}{\partial x}, \frac{\partial}{\partial y}, \frac{\partial}{\partial z}\right)$ . So, effectively an atom resides in a potential  $U_L \sim I(\mathbf{r})$ , where  $I(\mathbf{r}) \sim \mathbf{E}^2(\mathbf{r})$  is

the intensity of the electric field. By changing the intensity dependence, the behavior of the atom can be influenced.

Consider the following system. The atom has two levels, ground  $|g\rangle$  and excited  $|e\rangle$ , and the energy difference between them is  $\hbar\omega_0$ . The laser frequency is  $\omega_L$ . If the detuning is defined as  $\delta = \omega_L - \omega_0$ , it is possible to obtain the effective potential (for more information see [32, 60]):

$$V_L(\mathbf{r}) = \frac{3\pi c^2 \Gamma}{2\omega_0^3} \frac{I(\mathbf{r})}{\delta}, \quad (2.18)$$

where  $c$  is the speed of light,  $\Gamma$  is the decay rate of the excited state, and  $I(\mathbf{r})$  is the intensity of the laser light. The potential is proportional to the intensity, but depending on the sign of the detuning  $\Delta$ , it can have a plus or minus sign. Thus, the atoms condense in the minimum of the potential  $V_L(\mathbf{r})$  or, depending on the sign of  $\delta$ , in the minima or maxima of the potential  $I(\mathbf{r})$ . The lifetime of atoms in such a system is defined via the scattering rate [32]

$$\Gamma_{sc}(\mathbf{r}) = \frac{3\pi c^2}{2\hbar\omega_0^3} \left(\frac{\Gamma}{\Delta}\right)^2 I(\mathbf{r}). \quad (2.19)$$

For  $\delta \ll \Gamma$  the atoms are stable in the potential and it is possible to conduct experiments with them.

To create the lattice in one direction, two overlapping laser beams are needed. They form a standing wave, which has the intensity  $I(\mathbf{r}) \sim \sin^2 k_L x$  and the potential

$$V_L = V_0 \sin^2 k_L x. \quad (2.20)$$

In 3D, similarly

$$V_L = V_0 (\sin^2 k_L x + \sin^2 k_L y + \sin^2 k_L z). \quad (2.21)$$

Here  $k_L = \frac{2\pi}{\lambda}$  is the wave vector of the laser light. The wave vector  $k_L$  also defines the so-called recoil energy  $E_{recoil} = \frac{\hbar^2 k_L^2}{2m}$ , where  $m$  is the atom mass. The recoil energy is a natural experimental energy unit in the lattice, as it is the kinetic energy of the atom if it is moving with the momentum of the photon  $k_L$ .

In the nodes of the sin function (maxima or minima depending on the detuning), the potential  $V_L$  can be approximated as a harmonic trap

$$V \sim \left( \frac{\omega_x x^2}{2} + \frac{\omega_y y^2}{2} + \frac{\omega_z z^2}{2} \right). \quad (2.22)$$

These nodes are called lattice sites and this is how the lattice is created. Atoms are kept in the lattice sites, and may jump (hop) between neighboring sites.

Additionally, an external trapping potential of the form  $V_{trap} = \frac{m\omega_{trap}^2 x^2}{2}$  can be applied.

### 2.1.5 Hamiltonian in a lattice

Starting from the initial Hamiltonian of Equation 2.7 and using the lowest band approximation, the lattice Hamiltonian can be obtained [61]:

$$H = -\sum_{ij,s} J_{ij,s} \hat{b}_{i,s}^\dagger \hat{b}_{j,s} + \frac{1}{2} \sum_{ijkl,s} U_{ijkl,s} \hat{b}_{i,s}^\dagger \hat{b}_{j,s}^\dagger \hat{b}_{k,s} \hat{b}_{l,s} + \sum_{ij,s} V_{ij,s} \hat{b}_{i,s}^\dagger \hat{b}_{j,s}, \quad (2.23)$$

where

$$J_{ij,s} = -\int d\mathbf{x} w_s^{(0)}(\mathbf{x} - \mathbf{x}_i) \left( -\frac{\hbar^2 k^2}{2m_s} - \mu_s \right) w_s^{(0)}(\mathbf{x} - \mathbf{x}_j) \quad (2.24)$$

$$V_{ij,s} = \int d\mathbf{x} w_s^{(0)}(\mathbf{x} - \mathbf{x}_i) V_{s,ext}(\mathbf{r}) w_s^{(0)}(\mathbf{x} - \mathbf{x}_j) \quad (2.25)$$

$$U_{ijkl,s} = g \int d\mathbf{x} w_{s_i}^{(0)}(\mathbf{x} - \mathbf{x}_i) w_{s_j}^{(0)}(\mathbf{x} - \mathbf{x}_j) w_{s_k}^{(0)}(\mathbf{x} - \mathbf{x}_k) w_{s_l}^{(0)}(\mathbf{x} - \mathbf{x}_l). \quad (2.26)$$

Here  $V_{s,ext}(\mathbf{r})$  contains both the lattice potential of Equation 2.21 and the external trap (if any),  $\hat{b}_{i,s}^\dagger$  and  $\hat{b}_{i,s}$  are annihilation and creation operators for particles at site  $i$  with spin  $s$ . The intensity of the laser light is connected with  $V_{s,ext}(\mathbf{r})$  as in Equation 2.18. Here  $w_s^{(0)}(\mathbf{x} - \mathbf{x}_i)$  are Wannier functions, where  $\mathbf{x}_i$  is the coordinate of the lattice site  $i$ ,  $s = \uparrow, \downarrow$  is spin, (0) marks the lowest band Wannier function and the physical meaning of  $w_s^{(0)}(\mathbf{x} - \mathbf{x}_i)$  is wave function of the atom situated in lattice site  $i$ . The coefficients  $U, J$  are connected with the initial parameters of the lattice, for example with the intensity of laser light [32].

Assuming that the hopping  $J_{ij,s}$  and the interaction  $U_{ijkl,s}$  coefficients do not depend on the lattice site and hopping happens only between the nearest neighbors, Equation 2.23 gives the Hubbard Hamiltonian [62–65], which for a 1D system is

$$\hat{H} = -J \sum_i \left( \hat{a}_i^\dagger \hat{a}_{i+1} + \hat{a}_{i+1}^\dagger \hat{a}_i \right) + \frac{U}{2} \sum_i \hat{n}_i (\hat{n}_i - 1) + \sum_i \epsilon_i \hat{n}_i \quad (2.27)$$

for bosons and

$$\hat{H} = -J \sum_{i,s=\{\uparrow\downarrow\}} \left( \hat{c}_{i,s}^\dagger \hat{c}_{i+1,s} + \hat{c}_{i+1,s}^\dagger \hat{c}_{i,s} \right) + \frac{U}{2} \sum_i \hat{n}_{i,\uparrow} \hat{n}_{i,\downarrow} + \sum_{i,s} \epsilon_{i,s} \hat{n}_{i,s} \quad (2.28)$$

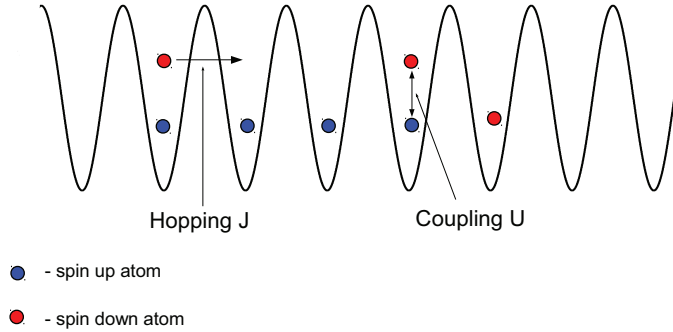


**Figure 2.3.** Ultracold atoms with different spins in a lattice. Blue color marks atoms with spin up, red with spin down. An atom hopping from one neighboring site to another is shown by a horizontal arrow. Coupling causing a shift in energy if two atoms with different spins are situated on the same lattice site is shown by a vertical, double-headed arrow.

for two-component fermions. A lattice is schematically shown in Figure 2.3. Here  $J$  is the tunnel coupling (responsible for kinetic energy),  $U$  is the on-site pair coupling (responsible for creating pairs) and  $\epsilon_i$  (or  $\epsilon_{i,s}$ ) is the trapping potential including other one-particle energies. The operators  $\hat{a}_i^\dagger$  and  $\hat{a}_i$  are bosonic creation and annihilation operators at lattice site  $i$ ,  $\hat{c}_{i,s}^\dagger$  and  $\hat{c}_{i,s}$  create and destroy a fermion at site  $i$  with spin  $s$ ,  $\hat{n}_i = \hat{a}_i^\dagger \hat{a}_i$  is the bosonic density at lattice site  $i$ , and  $\hat{n}_{i,s} = \hat{c}_{i,s}^\dagger \hat{c}_{i,s}$  is the density of fermions with spin  $s$  at site  $i$ . Equations  $[\hat{a}_i, \hat{a}_{i'}^\dagger] = \delta_{i,i'}$  for bosons and  $\{\hat{c}_{i,s}, \hat{c}_{i',s'}^\dagger\} = \delta_{i,i'} \delta_{s,s'}$  for fermions are satisfied too. In Equation 2.27, the pair coupling term  $\frac{U}{2} \sum_i \hat{n}_i (\hat{n}_i - 1)$  includes  $(\hat{n}_i - 1)$  to exclude the interaction of a particle with itself.

## 2.2 BCS theory and superfluidity

Superfluidity, including both usual Bardeen-Cooper-Schrieffer (BCS) type superconductivity and exotic form of superfluidity such as the Fulde-Ferrell-Larkin-Ovchinnikov (FFLO) state, are central in this thesis. Here, the basic definition of a Cooper pair is first presented, then more complicated issues, such as exotic superfluidity are considered.

### 2.2.1 Cooper pairs

In 1956, Cooper [66] predicted an instability in normal metal, which was later called after his name: the Cooper instability. He assumed that electrons fill the Fermi sphere, so that their distribution is a step-function  $n_F(\mathbf{k}) = \theta(|\mathbf{k}| < k_F)$ . He also assumed that interaction between electrons happens only in a narrow region near the Fermi surface (for more information see [67]):

$$V_{Cooper}(\mathbf{q}, \omega) = \begin{cases} -V_0, & \left| \frac{\hbar^2 \mathbf{q}^2}{2m} - E_F \right| < \hbar\omega_D \\ 0, & \left| \frac{\hbar^2 \mathbf{q}^2}{2m} - E_F \right| > \hbar\omega_D \end{cases}, \quad (2.29)$$

where  $E_F$  is the Fermi energy and  $\hbar\omega_D$  is the so-called Debye energy. The scattering amplitude between two electrons with opposite spins and momenta (e.g. in states  $(\uparrow, \mathbf{k})$  and  $(\downarrow, -\mathbf{k})$ ) is diverging for such a potential, which means that electrons form a bound state or a Cooper pair (Figure 2.4). When all electrons are paired with their counterparts, the metal is superconducting. The essential point is that the pairing happens for any value of  $V_0$ , that is even for a vanishingly small interaction.

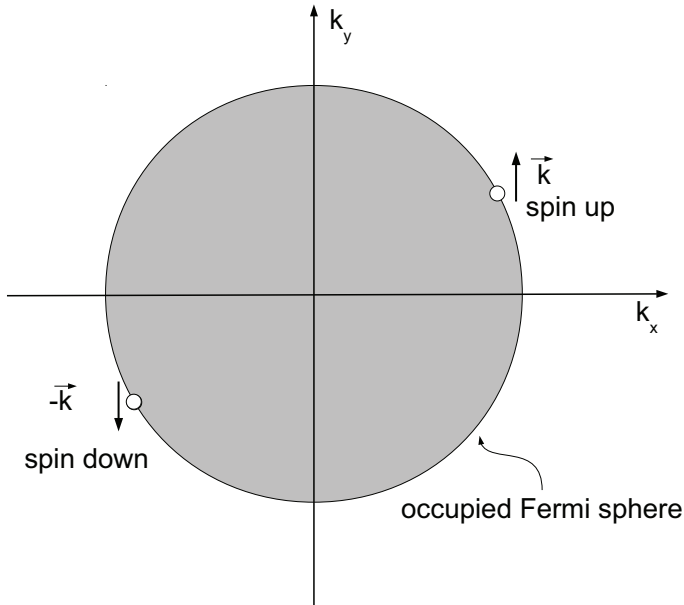


**Figure 2.4.** BCS pairing. The figure shows two atoms with opposite spins and momenta which are paired in the Cooper pair. The atoms inside the Fermi sphere create Cooper pairs too, but the strongest physical effect comes from the Cooper pairs with atom momenta close to the Fermi surface.

Cooper pairing can be described via a correlation function and here we intro-

duce the main quantity of BCS theory [68]: a pairing field

$$\langle \psi_{\downarrow}(\mathbf{r}, t) \psi_{\uparrow}(\mathbf{r}, t) \rangle = \Delta(\mathbf{r}, t), \quad (2.30)$$

which is non-zero when pairing exists. In a uniform case, the pairing field is constant  $\Delta(\mathbf{r}, t) = \Delta_0$ , but for the case of exotic superfluidity (examined in more detail in Subsection 2.2.2),  $\Delta$  shows non-uniform behavior.

The Hamiltonian with the interaction term given in Equation 2.29 is

$$H = \sum_{\mathbf{p}s} \left( \frac{\hbar^2 \mathbf{p}^2}{2m} - \mu \right) c_{\mathbf{p},s}^{\dagger} c_{\mathbf{p},s} + \sum_{\mathbf{q}\mathbf{p}\mathbf{p}'s's'} V_{Cooper}(\mathbf{q}) c_{\mathbf{p}+\mathbf{q},s}^{\dagger} c_{\mathbf{p}'-\mathbf{q},s}^{\dagger} c_{\mathbf{p}'s'} c_{\mathbf{p}s}, \quad (2.31)$$

where  $\mu$  is a chemical potential.

For Hamiltonian 2.31 in the mean-field approximation, the Green's function (which is a correlator of two operators, discussed more in Section 3.3 ) is [67]

$$G_s(p) = \frac{u_p^2}{ip - E_p} + \frac{v_p^2}{ip + E_p} \quad (2.32)$$

for  $s = \downarrow, \uparrow$ , where

$$E_p = \sqrt{\left( \frac{\hbar^2 p^2}{2m} - \mu \right)^2 + \Delta^2(p)}. \quad (2.33)$$

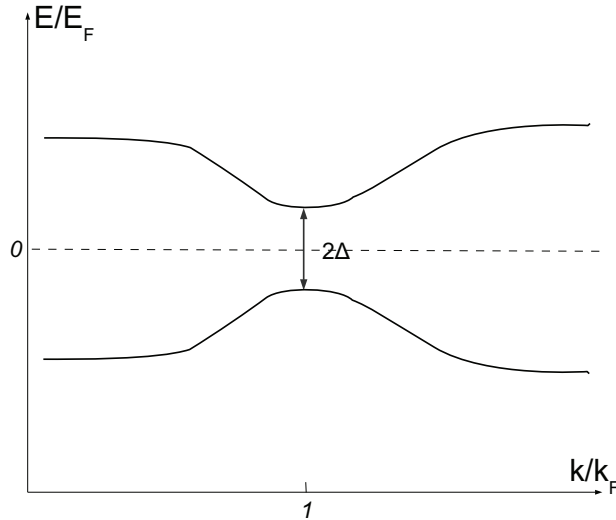


**Figure 2.5.** Quasiparticle energy levels for the Cooper pairs case for constant gap  $\Delta$  and  $\mu = E_F$ , where  $k_F$  is Fermi momentum and  $E_F$  is Fermi energy. The upper curve shows energy of quasiparticles of Equation 2.33 with the plus sign, the lower curve: with the minus sign. Close to the Fermi surface ( $p = 0$ ), the distance between the two levels is exactly  $2\Delta(p)$ .

The Green's function  $G_s(p)$  implies the existence of quasiparticles with energies  $\pm E_p$ . The pairing field  $\Delta$  can thus be seen as opening an excitation gap in the energy spectrum. Hence  $\Delta$  is often also called 'the gap'. In creating an excitation (that is, a particle and a hole), the smallest possible excitation energy is  $2\Delta(p)$ , or twice the gap (this can be seen in Figure 2.5). This minimal energy is one of the important causes of superfluidity/superconductivity (c.f. the Landau criterion [69]). If electrons (or other fermions) are already in a state with a non-zero gap, the critical velocity of the flow in the system is  $v_{cr} = \min_{\mathbf{p}} \frac{\varepsilon(\mathbf{p})}{|\mathbf{p}|}$ . Quasiparticles can be created only if the velocity of the flow is higher than the critical velocity  $v_{cr}$ . Here,  $\varepsilon(\mathbf{p})$  is energy dispersion for all values of  $\mathbf{p}$ , which is non-zero for non-zero gap; thus, for a non-zero gap, the critical velocity is non-zero.

For ultracold gases, similar reasoning also leads to superfluidity. However, for ultracold gases, instead of potentials such as Cooper potential  $V_{Cooper}$ , a simpler contact potential  $V(\mathbf{r}_1, \mathbf{r}_2) = g\delta(\mathbf{r}_1 - \mathbf{r}_2)$  can be used. Especially, in atomic gases the interactions can be attractive or repulsive depending on the choice of the hyperfine states or the magnetic field. Contrary to superconductors, in ultracold gases there is no need for phonon coupling for achieving attraction between the atoms.

### 2.2.2 Imbalanced gas

Earlier, a balanced gas was described where numbers of up and down particles are equal  $N_\uparrow = N_\downarrow$ . But imbalanced gases ( $N_\uparrow > N_\downarrow$ ) are also extremely interesting. For imbalanced gas the majority component is here chosen as the 'up' particle. The measure of how imbalanced the gas is is the polarization [70, 71]:

$$P = \frac{N_\uparrow - N_\downarrow}{N_\uparrow + N_\downarrow}. \quad (2.34)$$

The value of the polarization  $P$  is always between zero and one, or  $1 \geq P \geq 0$ . The case of  $P = 0$  is a balanced gas and the case of  $P = 1$  is a gas which consists only of up component atoms.

The special case of  $N_\downarrow = 1, N_\uparrow > 1$  corresponds to an impurity, which in the interacting case may create an excitation called polaron [49, 50, 72–74, 74–79]. If one minority particle is surrounded by the cloud of majority particles, the former creates strong bonds with the latter. These bonds contain some energy, which depends on the interaction  $U$  between the majority and minority particles. For zero interaction  $U = 0$ , bonds are not formed and a polaron does not exist. Thus, the energy of a polaron is defined as  $E_U - E_{U=0}$ , where  $E_U$  is the

total energy of the system for interaction  $U$ .

In publication IV it was investigated how the energy of a polaron in a 1D lattice with a trap changes for different interactions  $U$ .

### 2.2.3 The FFLO state and exotic superfluidity

Atoms which form Cooper pairs in the balanced gas have opposite momenta  $\mathbf{k}$  and  $-\mathbf{k}$ . Thus the total momentum of a Cooper pair is zero. This is the most energetically favourable configuration for a balanced gas ( $N_{\uparrow} = N_{\downarrow}$ ). But in an imbalanced gas, one may predict Cooper pairs with non-zero total momentum  $\mathbf{q}$ . Atoms inside such a Cooper pair have opposite spins  $\uparrow$  and  $\downarrow$ , but their momenta are  $\mathbf{k} + \mathbf{q}$  and  $-\mathbf{k}$ . This effect is caused by non-coinciding Fermi spheres.

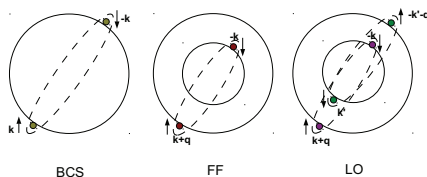


**Figure 2.6.** Comparison of BCS, FF and LO pairing. In case of BCS two atoms with opposite spins and momenta form the Cooper pair. In case of FF and LO states the spins are opposite, but momenta are not: this leads to non-zero total momenta. The difference between FF and LO states is that for FF the atoms are paired to form a total momentum  $\mathbf{q}$ , and for LO both  $\mathbf{q}$  and  $-\mathbf{q}$ .

Figure 2.6 shows how the atoms are paired. In the case of BCS pairing, atoms on the opposite sides of Fermi sphere are paired. In the imbalanced case one Fermi sphere is smaller in size than the other. Two possibilities of pairing in such a case have been introduced to the scientific community almost simultaneously: the FF phase by Fulde and Ferrell [80] and the LO phase by Larkin and Ovchinnikov [81]. In the FF case, Cooper pairs have a total momentum  $\mathbf{q}$ ; in the LO case, Cooper pairs have a total momentum of  $\mathbf{q}$  or  $-\mathbf{q}$ . In general, exotic superfluidity with non-zero total momenta of Cooper pairs is called the FFLO phase. Additionally, there are predictions such as the breached pair or Sarma state [82] and also states with a deformed Fermi surface [83], but they will not be considered in this thesis. Recently, there has been a lot of theoretical research concerning the possibility of the FFLO state in ultracold gases [71, 84–90].

As Cooper pairs have a momentum  $\mathbf{q}$ , the translational invariance of the system is broken. The gap is not uniform anymore and it oscillates with the wavelength  $\frac{2\pi}{q}$ . For the FF state, the gap is

$$\Delta(\mathbf{r}) \propto \Delta e^{-i\mathbf{q}\mathbf{r}}. \quad (2.35)$$

For the LO state the gap is following:

$$\Delta(\mathbf{r}) \propto \Delta \cos(\mathbf{q}\mathbf{r}). \quad (2.36)$$

In real systems, exotic superfluidity includes states with different  $\mathbf{q}$ :

$$\Delta(\mathbf{r}) \propto \sum_{\mathbf{q}} \Delta_{\mathbf{q}} e^{-i\mathbf{q}\mathbf{r}}. \quad (2.37)$$

The FFLO state is of special interest, as it has not been experimentally observed yet. In Publication I a method is suggested to identify the FFLO state using the lattice modulation spectroscopy for a gas in a lattice.

### 3. Density response

The collective excitation spectrum of a physical system gives a lot of important information about it. Calculating the collective mode frequencies of a many-body quantum system is in general highly non-trivial. There are multiple ways of searching for the resonances, and here the use of the density response function is considered. The density response is a function of frequency, defined in such a way that the peaks in it mark the resonant frequencies. In this Chapter the density response function will be introduced in detail. Another way of observing the resonant frequencies by modulating the amplitude of a lattice system will be discussed in the Chapter 4.

These calculations are motivated by experimental works where the frequencies of the collective excitations for different types of perturbations of the ultracold gas systems have been measured [91–94]. As the hydrodynamic theory has been unable to fully explain the experimental findings [40, 95, 96] it is of interest to consider other approaches. The RPA approximation and the BdG theory (see e.g. [97–99]) are used in order to describe the interesting intermediately strong interaction regime.

#### 3.1 General theory of the response function

Let us imagine a system with the Hamiltonian  $\hat{H}_0$  and that this system is perturbed by a small field,  $\hat{V}$ . The external perturbation influences the system and by measuring the results of this influence the information about the system can be gathered. Let us assume that the perturbation starts to act at the moment  $t = 0$ . Thus before  $t = 0$  the evolution of the system followed the Hamiltonian  $\hat{H}_0$  and after  $t = 0$  it is determined by the perturbed Hamiltonian  $\hat{H}_0 + \hat{V}$ . Let us assume that at the moment  $t = 0$  system is in the ground state  $|\phi_0\rangle$ . The state of the system at the moment of time  $t$  can be obtained from the Schrödinger equation

$$i\hbar \frac{\partial}{\partial t} |\phi(t)\rangle = (\hat{H}_0 + \hat{V}) |\phi(t)\rangle, \quad (3.1)$$

where the initial state  $|\phi(t=0)\rangle = |\phi_0\rangle$  satisfies

$$\hat{H}_0 |\phi_0\rangle = E_0 |\phi_0\rangle. \quad (3.2)$$

At the time  $t$  an observable is measured defined by a quantum operator  $\hat{O}(\mathbf{r})$ . According to the definition of the quantum observable operator  $O(\mathbf{r}, t)$  is

$$O(\mathbf{r}, t) = \langle \phi(t) | \hat{O}(\mathbf{r}) | \phi(t) \rangle. \quad (3.3)$$

Without the perturbation ( $\hat{V} = 0$ )  $|\phi(t)\rangle = |\phi_0\rangle$  (as  $|\phi_0\rangle$  is the ground state) and the result of measuring  $\hat{O}(\mathbf{r})$  will be

$$O_0(\mathbf{r}) = \langle \phi_0 | \hat{O}(\mathbf{r}) | \phi_0 \rangle. \quad (3.4)$$

The difference between  $O(\mathbf{r}, t)$  and  $O_0(\mathbf{r})$  is a measure of how much the perturbation has changed the system. Thus operator  $O(\mathbf{r}, t)$  is defined as

$$\delta O(\mathbf{r}, t) = O(\mathbf{r}, t) - O_0(\mathbf{r}), \quad (3.5)$$

which indicates how much the perturbation  $\hat{V}$  has influenced the expectation value of the observable  $\hat{O}$ .

In the interaction picture representation, in the linear order of  $\hat{V}$ , the wave function evolves as:

$$|\phi(t)\rangle_I = |\phi_0\rangle - i \int_{-\infty}^t dt' \hat{V}_I(t') |\phi_0\rangle + O(\hat{V}^2), \quad (3.6)$$

where  $\hat{V}_I$  is  $\hat{V}$  in the interaction picture representation:  $\hat{V}_I(t') = e^{i\hat{H}_0 t'} \hat{V} e^{-i\hat{H}_0 t'}$ . The expectation value of an operator  $\hat{O}(\mathbf{r})$  in the interaction picture representation  $O(\mathbf{r}, t) = \langle \phi(t) |_I \hat{O}_I(\mathbf{r}) | \phi(t) \rangle_I$  in the linear order on  $\hat{V}$  will be

$$O(\mathbf{r}, t) = \langle \phi_0 | \hat{O}_I(\mathbf{r}) | \phi_0 \rangle - i \int_{-\infty}^t dt' (\langle \phi_0 | \hat{O}_I(\mathbf{r}) \hat{V}_I(t') | \phi_0 \rangle - \langle \phi_0 | \hat{V}_I(t') \hat{O}_I(\mathbf{r}) | \phi_0 \rangle). \quad (3.7)$$

The first term on the right side of the equation is exactly the observable  $\hat{O}(\mathbf{r})$  measured in the absence of perturbation, or  $O_0(\mathbf{r})$ ; and with the help of Equation 3.5 one obtains

$$\delta O(\mathbf{r}, t) = -i \int_{-\infty}^t dt' (\langle \phi_0 | \hat{O}_I(\mathbf{r}) \hat{V}_I(t') | \phi_0 \rangle - \langle \phi_0 | \hat{V}_I(t') \hat{O}_I(\mathbf{r}) | \phi_0 \rangle) \quad (3.8)$$

or

$$\delta O(\mathbf{r}, t) = -i \int_{-\infty}^t dt' \langle \phi_0 | [\hat{O}_I(\mathbf{r}, t), \hat{V}_I(t')] | \phi_0 \rangle, \quad (3.9)$$

where  $\hat{O}_I$  and  $\hat{V}_I$  are the operators  $\hat{O}$  and  $\hat{V}$  in the interaction picture representation. A commonly used observable is the density  $\hat{O}(\mathbf{r}) = \hat{\rho}(\mathbf{r})$ , in which case the result is called 'the density response function', otherwise the general name is 'the response function'.

Often the potential  $\hat{V}$  is of the form

$$\hat{V} = \int d\mathbf{r} \hat{W}(\mathbf{r}) v(\mathbf{r}, t). \quad (3.10)$$

Then  $\delta O(\mathbf{r}, t)$  is

$$\delta O(\mathbf{r}, t) = -i \int_{-\infty}^t dt' \int d\mathbf{r}' \langle \phi_0 | [\hat{O}_I(\mathbf{r}, t), \hat{W}_I(\mathbf{r}', t')] | \phi_0 \rangle v(\mathbf{r}', t'), \quad (3.11)$$

where  $\hat{W}_I$  is the operator  $\hat{W}$  in the interaction picture representation. The retarded response function  $\mathcal{A}(\mathbf{r}, \mathbf{r}', t, t')$  is defined as the kernel of this expression

$$\delta O(\mathbf{r}, t) = \int_{-\infty}^{+\infty} dt' d\mathbf{r}' \mathcal{A}(\mathbf{r}, \mathbf{r}', t, t') v(\mathbf{r}', t'), \quad (3.12)$$

or

$$\mathcal{A}(\mathbf{r}, \mathbf{r}', t, t') = -i \langle \phi_0 | [\hat{O}_I(\mathbf{r}, t), \hat{W}_I(\mathbf{r}', t')] | \phi_0 \rangle \theta(t - t'). \quad (3.13)$$

Physically the perturbation of the density is often the simplest to implement, then  $\hat{W} = \hat{\rho}$  where  $\hat{\rho}$  is the density operator. Also the density is often the simplest observable to be measured, thus  $\hat{O} = \hat{\rho}$  also. In this special case the expression is:

$$\mathcal{A}(\mathbf{r}, \mathbf{r}', t - t') = -i \langle \phi_0 | [\hat{\rho}_I(\mathbf{r}, t), \hat{\rho}_I(\mathbf{r}', t')] | \phi_0 \rangle \theta(t - t'). \quad (3.14)$$

Thus for calculating  $\mathcal{A}(\mathbf{r}, \mathbf{r}', t - t')$  one needs to know the correlator  $\langle \phi_0 | [\hat{\rho}_I(\mathbf{r}, t), \hat{\rho}_I(\mathbf{r}', t')] | \phi_0 \rangle$ , which is not at all a trivial expression because of the interaction picture representation  $\hat{\rho}_I(\mathbf{r}, t) = e^{-i\hat{H}_0 t} \hat{\rho}(\mathbf{r}) e^{i\hat{H}_0 t}$ . However, in the next Section it will be shown how the density response can be calculated.

### 3.2 Collective frequencies in the response function

Equation 3.14 is already enough for calculating the density response function. But as only the frequencies of the modes are interesting, the more appropriate

form is the Fourier transform of Equation 3.14

$$\mathcal{A}(\mathbf{r}, \mathbf{r}', \omega) = -i \int_{-\infty}^0 dt'' e^{-i\omega t''} \langle \phi_0 | [\hat{\rho}_I(\mathbf{r}, 0), \hat{\rho}_I(\mathbf{r}', t'')] | \phi_0 \rangle. \quad (3.15)$$

Let us assume that the Hamiltonian  $\hat{H}_0$  is diagonalized with the eigenvalues  $E_n$  and the eigenvectors  $|n\rangle$ , thus

$$\hat{H}_0 |n\rangle = E_n |n\rangle, \quad n = 0, 1, \dots \quad (3.16)$$

As  $\hat{H}_0$  is a Hermitian operator, the eigenvectors are orthogonal  $\langle n | n' \rangle = \delta_{n, n'}$  and form a complete basis  $\sum_n |n\rangle \langle n| = \hat{1}$ . The ground state which earlier was called  $|\phi_0\rangle$ , will now correspond to the state with  $n = 0$ , or  $|\phi_0\rangle \equiv |0\rangle$ .

By expanding Equation 3.15 in the basis of the vectors  $|n\rangle$  and using  $e^{-i\hat{H}_0 t} |n\rangle = e^{-iE_n t} |n\rangle$  one obtains

$$\begin{aligned} \mathcal{A}(\mathbf{r}, \mathbf{r}', \omega) = & -i \int_{-\infty}^0 dt'' e^{-i\omega t''} \sum_n \left( e^{i(E_n - E_0)t''} \langle \phi_0 | \hat{\rho}(\mathbf{r}) | n \rangle \langle n | \hat{\rho}(\mathbf{r}') | \phi_0 \rangle \right. \\ & \left. - e^{i(E_0 - E_n)t''} \langle \phi_0 | \hat{\rho}(\mathbf{r}') | n \rangle \langle n | \hat{\rho}(\mathbf{r}) | \phi_0 \rangle \right). \end{aligned} \quad (3.17)$$

After integrating over time (a convergence factor  $i\eta$  is added to the energies) the final equation is

$$\mathcal{A}(\mathbf{r}, \mathbf{r}', \omega) = \sum_n \frac{\langle \phi_0 | \hat{\rho}(\mathbf{r}) | n \rangle \langle n | \hat{\rho}(\mathbf{r}') | \phi_0 \rangle}{\omega - (E_n - E_0)} - \frac{\langle \phi_0 | \hat{\rho}(\mathbf{r}') | n \rangle \langle n | \hat{\rho}(\mathbf{r}) | \phi_0 \rangle}{\omega + (E_n - E_0)}. \quad (3.18)$$

Considering the density response  $\mathcal{A}(\mathbf{r}, \mathbf{r}', \omega)$  as a function of  $\omega$ , it is possible to notice that the peaks of the response appear at the frequencies  $\omega = \omega_{n, \pm}$ , where

$$\omega_{n, \pm} = \pm (E_n - E_0). \quad (3.19)$$

As  $E_n - E_0$  are the energies of the transitions between the levels  $|n\rangle$  and  $|0\rangle$  (here  $\hbar = 1$ ), the frequencies  $\omega_{n, \pm}$  mark the excitations of the system, both collective and single particle. The system was initially in the state  $|0\rangle$ , so any transition from the initial state  $|0\rangle$  to a final state  $|n\rangle$  involves the energy  $\omega_{n, \pm}$ . The mathematical problem of finding the exact energies  $E_n$  (equivalent to diagonalization of Hamiltonian  $\hat{H}_0$ ) is practically impossible to solve for most many-body systems. However, calculating the density response function approximately is possible.

So by knowing the density response function  $\mathcal{A}(\mathbf{r}, \mathbf{r}', \omega)$  as a function of  $\omega$  one can easily reconstruct the (collective) frequencies of the excitations  $\omega_{n, \pm}$  as peaks of this function.

### 3.3 Linear density response

Let us consider the Hamiltonian  $\hat{H} = \hat{H}_{system} + \hat{V}_1 + \hat{V}_2$  and two perturbation fields  $\hat{V}_1$  and  $\hat{V}_2$  where

$$\begin{aligned} \hat{H}_{system} &= \sum_{\alpha} \int d\mathbf{r} \psi_{\alpha}^{\dagger}(\mathbf{r}) \left[ \frac{-\nabla^2}{2m} - \mu + \frac{m\omega^2 r^2}{2} \right] \psi_{\alpha}(\mathbf{r}) \\ &\quad + \frac{1}{2} g_0 \sum_{\alpha, \beta} \int d\mathbf{r} \psi_{\alpha}^{\dagger}(\mathbf{r}) \psi_{\beta}^{\dagger}(\mathbf{r}) \psi_{\alpha}(\mathbf{r}) \psi_{\beta}(\mathbf{r}) \\ &= \hat{H}_0 + \hat{H}_{int} \end{aligned} \quad (3.20)$$

$$\hat{V}_1 = \int d\mathbf{r} [\phi_{\uparrow}(\mathbf{r}, t) n_{\uparrow}(\mathbf{r}) + \phi_{\downarrow}(\mathbf{r}, t) n_{\downarrow}(\mathbf{r})] \quad (3.21)$$

$$\hat{V}_2 = \int d\mathbf{r} [\eta(\mathbf{r}, t) \psi_{\downarrow}(\mathbf{r}) \psi_{\uparrow}(\mathbf{r}) + \eta^*(\mathbf{r}, t) \psi_{\uparrow}^{\dagger}(\mathbf{r}) \psi_{\downarrow}^{\dagger}(\mathbf{r})]. \quad (3.22)$$

The external fields  $\phi_{\uparrow}(\mathbf{r}, t)$  and  $\phi_{\downarrow}(\mathbf{r}, t)$  are perturbations of the density up and down components in the point of the coordinates  $\mathbf{r}$  and  $t$ ,  $\eta(\mathbf{r}, t)$  is a perturbation of the pairing field. The Hamiltonian  $\hat{H}_{system}$  contains the standard kinetic energy and the two-particle interaction terms.

In such a system the time-ordered Green's function is defined as

$$\hat{G}(\mathbf{1}, \mathbf{2}) = -\langle T \Psi(\mathbf{1}) \Psi^{\dagger}(\mathbf{2}) \rangle, \quad (3.23)$$

where

$$\Psi(\mathbf{1}) = \begin{bmatrix} \psi_{\uparrow}(\mathbf{1}) \\ \psi_{\downarrow}^{\dagger}(\mathbf{1}) \end{bmatrix}, \quad \Psi^{\dagger}(\mathbf{2}) = \begin{bmatrix} \psi_{\uparrow}^{\dagger}(\mathbf{2}) & \psi_{\downarrow}(\mathbf{2}) \end{bmatrix} \quad (3.24)$$

and

$$\psi_{\gamma}(\mathbf{1}) = \psi_{\gamma}(\mathbf{x}_1, \tau_1) \quad (3.25)$$

and  $T$  is the time-ordering operator.

Also the Nambu-Gorkov form of the Green's function will be introduced:

$$\hat{G}(\mathbf{1}, \mathbf{2}) = \begin{pmatrix} G_{\uparrow}(\mathbf{1}, \mathbf{2}) & F(\mathbf{1}, \mathbf{2}) \\ F^*(\mathbf{2}, \mathbf{1}) & -G_{\downarrow}(\mathbf{2}, \mathbf{1}) \end{pmatrix}, \quad (3.26)$$

where  $G_{\uparrow}(\mathbf{1}, \mathbf{2})$  is the Green's function for a particles with spin up,  $G_{\downarrow}(\mathbf{2}, \mathbf{1})$  for particles with spin down and  $F(\mathbf{1}, \mathbf{2})$  is the pairing function, also called the anomalous Green's function, for which  $F(\mathbf{1}, \mathbf{1}) = \Delta(\mathbf{1})$ .

The Green's function describes the basic properties of the system and is the source of all information which is searched for. In particular, the density response function also can be extracted from the Green's functions. The Green's function is (by definition) the solution of the following equation:

$$\int d\mathbf{3}\hat{H}(\mathbf{1},\mathbf{3})\hat{G}(\mathbf{3},\mathbf{2}) = \delta(\mathbf{1}-\mathbf{2}), \quad (3.27)$$

and the same for the Green's function of the non-interacting Hamiltonian:

$$\int d\mathbf{3}\hat{H}_0(\mathbf{1},\mathbf{3})\hat{G}_0(\mathbf{3},\mathbf{2}) = \delta(\mathbf{1}-\mathbf{2}). \quad (3.28)$$

Starting from the definitions of Equations 3.27 and 3.28 one can show that functions  $\hat{G}$  and  $\hat{G}_0$  are connected by the Dyson equation

$$\hat{G}^{-1} = \hat{G}_0^{-1} - W - \Sigma, \quad (3.29)$$

where the self-energies are

$$W(\mathbf{3},\mathbf{4}) = \begin{pmatrix} \phi_{\uparrow}(\mathbf{3}) & \eta^*(\mathbf{3}) \\ \eta(\mathbf{3}) & \phi_{\downarrow}(\mathbf{3}) \end{pmatrix} \hat{\delta}(\mathbf{3}-\mathbf{4}) \quad (3.30)$$

$$\Sigma(\mathbf{3},\mathbf{4}) = g_0 \int d\mathbf{5} \begin{pmatrix} \langle T\psi_{\uparrow}^{\dagger}(\mathbf{5})n(\mathbf{3})\psi_{\uparrow}(\mathbf{3}) \rangle & \langle T\psi_{\downarrow}(\mathbf{5})n(\mathbf{3})\psi_{\uparrow}(\mathbf{3}) \rangle \\ -\langle T\psi_{\uparrow}^{\dagger}(\mathbf{5})\psi_{\downarrow}^{\dagger}(\mathbf{3})n(\mathbf{3}) \rangle & \langle T\psi_{\downarrow}^{\dagger}(\mathbf{3})n(\mathbf{3})\psi_{\downarrow}(\mathbf{5}) \rangle \end{pmatrix} \hat{G}^{-1}(\mathbf{5},\mathbf{4}), \quad (3.31)$$

and  $\hat{\delta}$  means a unitary operator.

As  $GG^{-1} = \hat{1}$ , one obtains

$$\frac{\delta\hat{G}(\mathbf{1},\mathbf{2})}{\delta h(\mathbf{3})} = - \int d\mathbf{3}d\mathbf{4}\hat{G}(\mathbf{1},\mathbf{3})\frac{\delta\hat{G}^{-1}(\mathbf{3},\mathbf{4})}{\delta h(\mathbf{5})}\hat{G}(\mathbf{4},\mathbf{2}), \quad (3.32)$$

and then using Equations 3.29 and 3.32 one can derive

$$\begin{aligned} \frac{\delta\tilde{G}(\mathbf{1},\mathbf{2})}{\delta h(\mathbf{5})} &= \tilde{A}_0(\mathbf{1},\mathbf{2},\mathbf{5}) + g_0 \int d\mathbf{3}\frac{\delta n(\mathbf{3})}{\delta h(\mathbf{5})}\tilde{G}(\mathbf{1},\mathbf{3})\tilde{G}(\mathbf{3},\mathbf{2}) \\ &\quad - g_0 \int d\mathbf{3}\tilde{G}(\mathbf{1},\mathbf{3})\frac{\delta\tilde{G}(\mathbf{3},\mathbf{3})}{\delta h(\mathbf{5})}\tilde{G}(\mathbf{3},\mathbf{2}), \end{aligned} \quad (3.33)$$

where

$$\tilde{A}_0(\mathbf{1},\mathbf{2},\mathbf{5}) = \tilde{G}(\mathbf{1},\mathbf{5})\frac{\delta W(\mathbf{5})}{\delta h(\mathbf{5})}\tilde{G}(\mathbf{5},\mathbf{2}) \quad (3.34)$$

and  $h$  can be of any of the fields  $\phi_{\uparrow}$ ,  $\phi_{\downarrow}$  or  $\eta$ . Here  $W(\mathbf{5})$  is marked as  $W(\mathbf{5}) = W(\mathbf{5},\mathbf{5})$ . All variables with tilde are usual operators multiplied by the Pauli matrix  $\tau_3 = \begin{pmatrix} 1 & 0 \\ 0 & -1 \end{pmatrix}$ , e.g.  $\tilde{G}(\mathbf{1},\mathbf{3}) = \tau_3\hat{G}(\mathbf{1},\mathbf{3})$ , where  $\hat{G}$  is a usual Green's function.

This multiplication does not influence the collective frequencies, but comes to compensate different signs for  $\hat{G}_{\uparrow\uparrow}$  and  $\hat{G}_{\downarrow\downarrow}$ .

One can extract the density response  $\frac{\delta\hat{\rho}(\mathbf{1})}{\delta h(\mathbf{3})}$  from the Green's function response  $\frac{\delta\hat{G}(\mathbf{1},\mathbf{2})}{\delta h(\mathbf{3})}$  when one notices that

$$\hat{G}(\mathbf{1},\mathbf{1}) = \begin{pmatrix} \rho_{\uparrow}(\mathbf{1}) & \Delta(\mathbf{1}) \\ \Delta(\mathbf{1}) & -\rho_{\downarrow}(\mathbf{1}) \end{pmatrix}, \quad (3.35)$$

where  $\rho_\uparrow$  and  $\rho_\downarrow$  are the densities of the up and down components, and  $\Delta$  is the gap. Thus if one calculates  $\left. \frac{\delta \tilde{G}(\mathbf{1}, \mathbf{2})}{\delta h(\mathbf{3})} \right|_{\mathbf{1}=\mathbf{2}}$ , one obtains not only the density response, but also additionally the response of the gap to the perturbation.

If the notation  $\tilde{A}_{ij}(\mathbf{1}, \mathbf{2}, \mathbf{5}) = \frac{\delta \tilde{G}_{ij}(\mathbf{1}, \mathbf{2})}{\delta h(\mathbf{5})}$  is used, then Equation 3.33 is a linear equation for  $\tilde{A}_{ij}$ :

$$\begin{aligned} \tilde{A}_{ij}(\mathbf{1}, \mathbf{2}, \mathbf{5}) &= \tilde{A}_{0ij}(\mathbf{1}, \mathbf{2}, \mathbf{5}) + g_0 \sum_{k,l} \int d\mathbf{3} \tilde{G}_{ik}(\mathbf{1}, \mathbf{3}) \tilde{G}_{kj}(\mathbf{3}, \mathbf{2}) \tilde{A}_{ll}(\mathbf{3}, \mathbf{3}, \mathbf{5}) \\ &\quad - g_0 \sum_{k,l} \int d\mathbf{3} \tilde{G}_{ik}(\mathbf{1}, \mathbf{3}) \tilde{G}_{lj}(\mathbf{3}, \mathbf{2}) \tilde{A}_{kl}(\mathbf{3}, \mathbf{3}, \mathbf{5}). \end{aligned} \quad (3.36)$$

Notice that the response function  $\tilde{A}_{ij}(\mathbf{1}, \mathbf{2}, \mathbf{5})$  involves time-ordered Green's function 3.23, whereas the response function from Equation 3.14 involves a retarded correlator. The two are closely connected as described in [59]. It is convenient also to use the notation

$$L_{iklj}(\mathbf{1}, \mathbf{2}, \mathbf{3}) = \tilde{G}_{ik}(\mathbf{1}, \mathbf{3}) \tilde{G}_{lj}(\mathbf{3}, \mathbf{2}) \quad (3.37)$$

and

$$\tilde{A}_{ij}(\mathbf{1}, \mathbf{5}) = \tilde{A}_{ij}(\mathbf{1}, \mathbf{2}, \mathbf{5}) \Big|_{\mathbf{1}=\mathbf{2}}. \quad (3.38)$$

The value  $\tilde{A}_{ij}(\mathbf{1}, \mathbf{5})$  is important as it directly gives the density and gap responses (remember Equation 3.35). Thus the main equation for the linear density response which will be used further is

$$\tilde{A}_{ij}(\mathbf{1}, \mathbf{5}) = \tilde{A}_{0ij}(\mathbf{1}, \mathbf{5}) + g_0 \sum_{k,l} \int d\mathbf{3} L_{ikkj}(\mathbf{1}, \mathbf{3}) \tilde{A}_{ll}(\mathbf{3}, \mathbf{5}) - g_0 \sum_{k,l} \int d\mathbf{3} L_{iklj}(\mathbf{1}, \mathbf{3}) \tilde{A}_{kl}(\mathbf{3}, \mathbf{5}), \quad (3.39)$$

where

$$L_{iklj}(\mathbf{1}, \mathbf{3}) = \tilde{G}_{ik}(\mathbf{1}, \mathbf{3}) \tilde{G}_{lj}(\mathbf{3}, \mathbf{1}) \quad (3.40)$$

and

$$\tilde{A}_0(\mathbf{1}, \mathbf{5}) = \tilde{G}(\mathbf{1}, \mathbf{5}) \frac{\delta W(\mathbf{5})}{\delta h(\mathbf{5})} \tilde{G}(\mathbf{5}, \mathbf{1}) \quad (3.41)$$

for the fields  $h = \phi_\uparrow, \phi_\downarrow, \eta$ .

For  $h = \phi_\uparrow$  the last equation gives

$$\tilde{A}_0(\mathbf{1}, \mathbf{5}) = \tilde{G}(\mathbf{1}, \mathbf{5}) \begin{pmatrix} 1 & 0 \\ 0 & 0 \end{pmatrix} \tilde{G}(\mathbf{5}, \mathbf{1}), \quad (3.42)$$

for  $h = \phi_\downarrow$  the result is

$$\tilde{A}_0(\mathbf{1}, \mathbf{5}) = \tilde{G}(\mathbf{1}, \mathbf{5}) \begin{pmatrix} 0 & 0 \\ 0 & 1 \end{pmatrix} \tilde{G}(\mathbf{5}, \mathbf{1}), \quad (3.43)$$

and for  $h = \phi_1$  the following is correct

$$\tilde{A}_0(\mathbf{1}, \mathbf{5}) = \tilde{G}(\mathbf{1}, \mathbf{5}) \begin{pmatrix} 0 & 0 \\ 1 & 0 \end{pmatrix} \tilde{G}(\mathbf{5}, \mathbf{1}). \quad (3.44)$$

### 3.4 Introducing the angular momentum

The spherical symmetry of the problem has not been yet utilized. First let us introduce the following decomposition

$$F(\mathbf{r}_1, \mathbf{r}_2) = \sum_L f_L(r_1, r_2) P_L(\cos \gamma), \quad (3.45)$$

where  $P_L(\cos \gamma)$  is a Legendre polynomial of a degree  $L$ . Here, instead of using the Cartesian coordinates where two points are marked by the Cartesian vectors  $\mathbf{r}_1, \mathbf{r}_2$ , the spherical coordinates where the same two points are marked by the scalar radii  $r_1, r_2$  and the angle  $\gamma$  between them are introduced. Any function of the two variables  $F(\mathbf{r}_1, \mathbf{r}_2)$  may be decomposed using Equation 3.45.

The decomposing of Equation 3.39, or (effectively) decomposing each of the variables which are used in that equation is needed. Before doing that, let us just check how the integration of a function in the Cartesian coordinates look like in terms of the decomposed coefficients. For that the so called 'addition theorem' will be needed for Legendre polynomials, namely:

$$P_L(\cos \gamma) = \frac{4\pi}{2L+1} \sum_{M=-L}^L Y_{LM}^*(\theta_1, \varphi_1) Y_{LM}(\theta_2, \varphi_2), \quad (3.46)$$

where  $Y_{LM}(\theta, \varphi)$  are the spherical harmonics. Thus using spherical harmonics any function can be decomposed similar to Equation 3.45:

$$F(\mathbf{r}_1, \mathbf{r}_2) = \sum_{LM} \frac{4\pi}{2L+1} f_{LM}(r_1, r_2) Y_{LM}^*(\theta_1, \varphi_1) Y_{LM}(\theta_2, \varphi_2). \quad (3.47)$$

The integration of two functions, decomposed as in Equation 3.47, will look like

$$\begin{aligned} & \int d\mathbf{r}_2 F(\mathbf{r}_1, \mathbf{r}_2) G(\mathbf{r}_2, \mathbf{r}_3) \\ &= \sum_{L_1 M_1 L_2 M_2} \frac{4\pi}{2L_1+1} \frac{4\pi}{2L_2+1} \left( \int r_2^2 dr_2 f_{L_1}(r_1, r_2) g_{L_2}(r_2, r_3) \right) \\ & \quad * \left( \int d\Omega_2 Y_{L_1 M_1}(\theta_2, \varphi_2) Y_{L_2 M_2}^*(\theta_2, \varphi_2) \right) Y_{L_1 M_1}^*(\theta_1, \varphi_1) Y_{L_2 M_2}(\theta_3, \varphi_3) \\ &= \sum_{LM} \left( \frac{4\pi}{2L+1} \right)^2 \left( \int r_2^2 dr_2 f_L(r_1, r_2) g_L(r_2, r_3) \right) Y_{LM}^*(\theta_1, \varphi_1) Y_{LM}(\theta_3, \varphi_3). \end{aligned} \quad (3.48)$$

So, if  $B(\mathbf{r}_1, \mathbf{r}_3) = \int d\mathbf{r}_2 F(\mathbf{r}_1, \mathbf{r}_2) G(\mathbf{r}_2, \mathbf{r}_3)$ , then its decomposition is

$$B(\mathbf{r}_1, \mathbf{r}_3) = \sum_{LM} \frac{4\pi}{2L+1} b_L(r_1, r_3) Y_{LM}^*(\theta_1, \varphi_1) Y_{LM}(\theta_3, \varphi_3), \quad (3.49)$$

where

$$b_L(r_1, r_3) = \left( \frac{4\pi}{2L+1} \right) \left( \int r_2^2 dr_2 f_L(r_1, r_2) g_L(r_2, r_3) \right). \quad (3.50)$$

Now this knowledge will be applied to Equation 3.39. The coefficients  $L_{iklj}(\mathbf{1}, \mathbf{3})$  and  $\tilde{A}_{ik}(\mathbf{1}, \mathbf{2})$  are decomposed according to the finite temperature Matsubara decomposition [67]:

$$L_{iklj}(\mathbf{1}, \mathbf{3}) = \frac{1}{\beta} \sum_{L,n} \mathcal{L}_{iklj,L}(r_1, r_3, \Omega_n) P_L(\cos \gamma) \exp(-i\Omega_n(t_1 - t_2)) \quad (3.51)$$

and

$$\tilde{A}_{ik}(\mathbf{1}, \mathbf{2}) = \frac{1}{\beta} \sum_{L,n} \mathcal{A}_{ik,L}(r_1, r_2, \Omega_n) P_L(\cos \gamma) \exp(-i\Omega_n(t_1 - t_2)). \quad (3.52)$$

Here  $\beta = \frac{1}{kT}$  is thermodynamic beta and  $\Omega_n = \frac{(2n+1)\pi}{\beta}$  are Matsubara frequencies. After this decomposition we move back from Matsubara frequencies to the usual ones and Equation 3.39 becomes

$$\begin{aligned} \mathcal{A}_{ij,L}(r_1, r_5, \omega) &= \mathcal{A}_{0ij,L}(r_1, r_5, \omega) \\ &+ g_0 \frac{4\pi}{2L+1} \sum_{k,l} \int r_3^2 dr_3 \mathcal{L}_{ikkj,L}(r_1, r_3, \omega) \mathcal{A}_{ll,L}(r_3, r_5, \omega) \\ &- g_0 \frac{4\pi}{2L+1} \sum_{k,l} \int r_3^2 dr_3 \mathcal{L}_{iklj,L}(r_1, r_3, \omega) \mathcal{A}_{kl,L}(r_3, r_5, \omega). \end{aligned} \quad (3.53)$$

Earlier the density response had a physically intuitive form:  $\tilde{A}_{ik}(\mathbf{1}, \mathbf{2})$  is the response of the density or the gap (controlled by indices  $ik$ ) at the point  $\mathbf{r}_1$  at the moment of time  $t_1$  if small point-like perturbation was applied at the point  $\mathbf{r}_2$  at the moment of time  $t_2$ . Now  $\mathcal{A}_{ij,L}(r_1, r_5, \omega)$  is a response of the density or gap (indices  $ij$ ) at the radius  $r_1$  if the excitation with the frequency  $\omega$  and the angular momentum  $L$  was applied at the radius  $r_5$ .

Due to the introduction of the angular momentum  $L$ , the numerical calculations are simplified a lot. This follows from the spherical symmetry of the underlying quantum system (the spherical symmetry of the Hamiltonian  $\hat{H}_0$ ). The perturbation  $\hat{V}$  does not need to be spherically symmetric and the model discussed here can describe well monopole ( $L = 0$ ), dipole ( $L = 1$ ) and quadrupole ( $L = 2$ ) modes. Still, calculating collective excitations for higher momenta  $L$  needs much more resources than the spherically symmetric case  $L = 0$ . For example, for the case  $L = 1$  the calculation is three times longer than for  $L = 0$ .

Note that in a very symbolic way one can rewrite Equation 3.53 as following

$$\mathcal{A}_{ij,L}(r_1, r_5, \omega) = \sum_{k,l} (1-K)_{ijkl}^{-1}(r_1, r_3, \omega) \mathcal{A}_{0kl,L}(r_3, r_5, \omega), \quad (3.54)$$

where matrix  $(1-K)$  is the kernel of Equation 3.53 and  $\hat{K}$  can be symbolically written as

$$\begin{aligned} K(r_1, r_3, \omega) = & g_0 \frac{4\pi}{2L+1} \int r_3^2 dr_3 \mathcal{L}_{ikkj,L}(r_1, r_3, \omega) \\ & - g_0 \frac{4\pi}{2L+1} \int r_3^2 dr_3 \mathcal{L}_{iklj,L}(r_1, r_3, \omega). \end{aligned} \quad (3.55)$$

As for us it is enough to know the mode frequencies, corresponding to the peaks in  $\mathcal{A}$ , the calculations can be simplified. Peaks (infinities) in  $\mathcal{A}$  happen when the matrix  $(1-K)$  has zero eigenvalues. So, instead of solving Equation 3.53, one can simply calculate the singular values of the matrix  $(1-K)$ . This can save computational resources. Both the density response and the singular values of the matrix  $(1-K)$  will be actually calculated, and the results will be compared.

Physically the random phase approximation (RPA) introduces interactions between the quasiparticles. In practice, this means including so called ring diagrams [59], which are not included in the mean-field theory. The method can thus describe physics not included in the static theory, such as the interactions between the quasiparticles. However, as a linear response theory it is valid only for small perturbations.

### 3.5 Bogolyubov-deGennes equations and density response

In the Subsection 2.1.3 the Bogolyubov-deGennes (BdG) equations were discussed. After performing a mean-field transformation the quadratic Hamiltonian can be diagonalized

$$\hat{H}_{MF} = \sum_{n,\alpha} E_n \gamma_{n\alpha}^\dagger \gamma_{n\alpha}, \quad (3.56)$$

where  $\gamma_{n\alpha}^\dagger$  and  $\gamma_{n\alpha}$  are the creation and annihilation operators of quasiparticles. Let us apply this knowledge for calculating the Green's function coefficients  $\mathcal{L}_{iklj,L}(r_1, r_3, \omega)$  and the Green's functions, as  $L_{iklj}(\mathbf{1}, \mathbf{3})$  is expressed via the Green's function (as shown in Equation 3.37).

First, let us connect the quasiparticle operators  $\gamma_{n\alpha}^\dagger, \gamma_{n\alpha}$  with the particle operators  $c_{n|m\uparrow}^\dagger, c_{n|m\uparrow}$  of the Hamiltonian 3.20 (here the results of applying the BdG theory to the special case of a harmonic trapping potential are used) [98, 100, 101]

$$c_{nlm\uparrow} = \sum_{j=1}^N W_{n,j}^l \gamma_{jlm\uparrow} + (-1)^m \sum_{j=1}^N W_{n,N+j}^l \gamma_{jlm\downarrow}^\dagger \quad (3.57)$$

$$c_{nlm\downarrow}^\dagger = (-1)^m \sum_{j=1}^N W_{N+n,j}^l \gamma_{jlm\downarrow}^\dagger + \sum_{j=1}^N W_{N+n,N+j}^l \gamma_{jlm\uparrow}. \quad (3.58)$$

Here  $W_{n,j}^l$  are the scalar coefficients, and the particle operators  $c_{nlm\downarrow}^\dagger, c_{nlm\uparrow}$  correspond to a state with an energy number  $n$ , the angular momentum  $l$  and z-projection of angular momentum  $m$  or

$$\psi_\alpha(\mathbf{r}) = \sum_{nlm} R_{nl}(r) Y_{lm}(\hat{\theta}) c_{nlm\alpha}. \quad (3.59)$$

Here  $Y_{lm}(\hat{\theta})$  are the spherical harmonics, and  $R_{nl}(r)$  are the radial eigenstates

$$R_{nl}(r) = \sqrt{2}(m\omega_T)^{3/4} \sqrt{\frac{n!}{(n+l+1/2)!}} e^{-\bar{r}^2/2} \bar{r}^l L_n^{l+1/2}(\bar{r}^2), \quad (3.60)$$

where  $L_n^{l+1/2}(\bar{r}^2)$  is the associated Laguerre polynomial and  $\bar{r} \equiv r \sqrt{\frac{m\omega_T}{\hbar}}$ ,  $\omega_T$  is the trap frequency.

After the Hamiltonian 3.20 is transformed to its mean-field form

$$H_{0,MF} = \sum_{\alpha=\{\uparrow,\downarrow\}} \int d\mathbf{r} \psi_\alpha^\dagger(\mathbf{r}) \left[ \frac{-\nabla^2}{2m} - \mu + \frac{m\omega_T^2 r^2}{2} \right] \psi_\alpha(\mathbf{r}) - \left( \int d\mathbf{r} \psi_\uparrow^\dagger(\mathbf{r}) \psi_\downarrow^\dagger(\mathbf{r}) \Delta(\mathbf{r}) + h.c. \right), \quad (3.61)$$

one can diagonalize it and find the coefficients  $W$ . The Green's function from Equation 3.23 with the help of Equations 3.24 and 3.59 looks as

$$\widehat{G}(\mathbf{1}, \mathbf{2}) = \sum_{nlm\downarrow, n'l'm'\downarrow} \begin{pmatrix} \langle c_{nlm\uparrow} c_{n'l'm'\uparrow}^\dagger \rangle & \langle c_{nlm\uparrow} c_{n'l'm'\downarrow} \rangle \\ \langle c_{nlm\downarrow}^\dagger c_{n'l'm'\uparrow} \rangle & \langle c_{nlm\downarrow}^\dagger c_{n'l'm'\downarrow} \rangle \end{pmatrix} R_{nl}(r_1) Y_{lm}(\hat{\theta}_1) R_{n'l'}(r_2) Y_{l'm'}(\hat{\theta}_2) e^{-i(E_{nlm}t_2 - E_{n'l'm'}t_1)} \quad (3.62)$$

or using again Matsubara decomposition

$$\widehat{G}(\mathbf{r}_1, \mathbf{r}_2, \Omega_n) = - \sum_{j,l} \frac{2l+1}{4\pi} P_l(\cos\theta_{12}) * \left( \Lambda_{jl}^-(r_1) \Lambda_{jl}^{-\dagger}(r_2) \frac{1}{i\Omega_n - E_{jl}} + \Lambda_{jl}^+(r_1) \Lambda_{jl}^{+\dagger}(r_2) \frac{1}{i\Omega_n + E_{jl}} \right), \quad (3.63)$$

where  $\Lambda_{jl}^-(r) = \sum_n \begin{pmatrix} W_{n,N+j}^l \\ W_{N+n,N+j}^l \end{pmatrix} R_{nl}(r)$ ,  $\Lambda_{jl}^+(r) = \sum_n \begin{pmatrix} W_{n,j}^l \\ W_{N+n,j}^l \end{pmatrix} R_{nl}(r)$ . Here  $P_l(\cos\theta_{12}) = \frac{4\pi}{2L+1} \sum_{M=-L}^L Y_{LM}^*(\theta_1, \varphi_1) Y_{LM}(\theta_2, \varphi_2)$  are the Legendre polynomials and  $\theta_{12}$  is the angle between the vectors  $\mathbf{r}_1$  and  $\mathbf{r}_2$ .

With such a Green's function and using Equation 3.37 and the decomposition 4.7, one can calculate the coefficients  $\mathcal{L}_{iklj,L}$  for Equation 3.53:

$$\begin{aligned} \mathcal{L}_{iklj,L}(r_1, r_3, \omega) = & (2L+1) \sum_{L_1 L_2} \begin{pmatrix} L & L_1 & L_2 \\ 0 & 0 & 0 \end{pmatrix}^2 \frac{2L_1+1}{4\pi} \frac{2L_2+1}{4\pi} \\ & * \sum_{J_1 J_2} \left( \lambda_{J_1 L_1, ik}^- \lambda_{J_2 L_2, lj}^- \frac{n_F(E_{J_1 L_1}) - n_F(E_{J_2 L_2})}{\omega + E_{J_1 L_1} - E_{J_2 L_2}} \right. \\ & + \lambda_{J_1 L_1, ik}^+ \lambda_{J_2 L_2, lj}^+ \frac{n_F(-E_{J_1 L_1}) - n_F(-E_{J_2 L_2})}{\omega - E_{J_1 L_1} + E_{J_2 L_2}} \\ & + \lambda_{J_1 L_1, ik}^- \lambda_{J_2 L_2, lj}^+ \frac{n_F(E_{J_1 L_1}) - n_F(-E_{J_2 L_2})}{\omega + E_{J_1 L_1} + E_{J_2 L_2}} \\ & \left. + \lambda_{J_1 L_1, ik}^+ \lambda_{J_2 L_2, lj}^- \frac{n_F(-E_{J_1 L_1}) - n_F(E_{J_2 L_2})}{\omega - E_{J_1 L_1} - E_{J_2 L_2}} \right). \end{aligned} \quad (3.64)$$

Here the occupation numbers are given by the Fermi-Dirac function  $n_F(E) = \frac{1}{\exp(\beta E) + 1}$  at the temperature  $k_B T = \frac{1}{\beta}$ . Furthermore,  $\begin{pmatrix} L & L_1 & L_2 \\ 0 & 0 & 0 \end{pmatrix}$  are the Wigner 3j-symbols. Finally,  $\lambda_{J_1 L_1, ik}^\pm = \Lambda_{J_1 L_1, i}^\pm(r_1) \Lambda_{J_1 L_1, k}^{\pm\dagger}(r_3)$  and  $\lambda_{J_2 L_2, lj}^\pm = \Lambda_{J_2 L_2, l}^\pm(r_3) \Lambda_{J_2 L_2, j}^{\pm\dagger}(r_1)$ .

Now, Equations 3.53 and 3.64 together give us enough information to calculate the response function  $\mathcal{A}_{ij,L}(r_1, r_5, \omega)$ .

### 3.6 Key results

The theory for the density response from the Sections 3.1-3.5 was used in order to calculate the frequencies of the collective excitations of a 3D spherically symmetrical two-component ultracold gas in a trap. The author started from the Hamiltonian 3.20 assuming attractive interaction, used the Equation 3.29, the simplified Equation 3.36 using the spherical symmetry and solved the Equation 3.53 using the Equation 3.64 for coefficients  $\mathcal{L}_{iklj,L}(r_1, r_3, \omega)$ . Those calculations were done for 4930 atoms in a 3D spherically symmetrical trap and considered only the angular momentum  $L = 0$ . The results of our research are presented in publication II and publication III; here the key findings are shortly summarized.

Publication II explores the gas in a spherically symmetric three-dimensional (3D) trap. The author starts from the random phase approximation and using the Bogolyubov-deGennes theory calculates the density response of a Fermi gas. Two quantities are studied: full density response  $A$ , peaks of which point out the frequencies of the collective excitations, and single particles density response  $A$ , peaks of which point out the frequencies of the single particle exci-

tations. The monopole mode (or zero angular momentum  $L = 0$ ) is studied. An interesting crossover is observed around  $k_F a \sim -0.8$  where  $k_F$  is Fermi momentum and  $a$  is scattering length;  $k_F a$  serves as measure of the interactions (for more information see Figure 3.1). For this crossover the pair vibration mode which starts from  $\omega = 0$  for  $k_F a = 0$  merges together with the collisionless hydrodynamic mode which starts from  $\omega = 2\omega_T$  for  $k_F a = 0$ . Near the merging also the pair vibration mode decreases its bandwidth (see figure 5 of publication II in the end of the thesis).

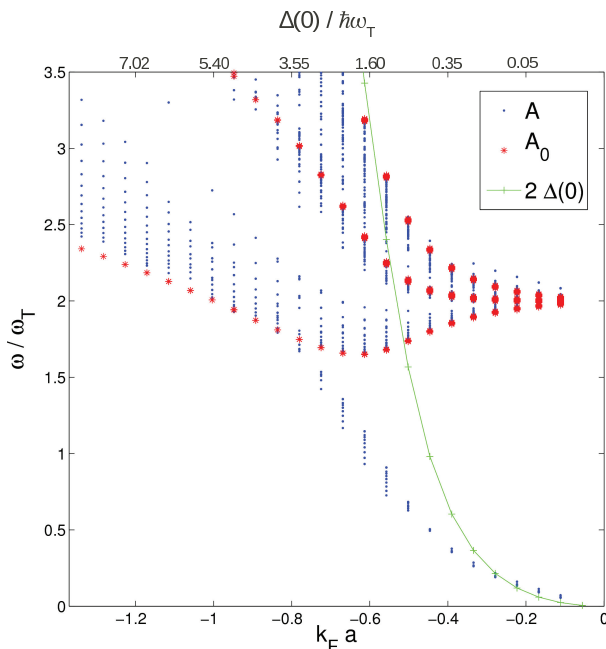


**Figure 3.1.** The peaks in the density responses as a function of the interaction  $k_F a$  or gap in the center of the trap  $\Delta(0)$ . Here  $A$  is the full density response, and  $A_0$  is the single particle density response as discussed in the text. Reproduced with permission from Publication II of this thesis.

In publication III as indicators for the collective excitations three quantities strength function (the density response as  $\mathcal{A}$  in the Equation 3.53), the lowest singular value of the matrix  $(1-K)$  (as discussed in the Subsection 3.4) and the logarithm of the determinant of the same matrix  $(1-K)$  (assuming that if one of the singular values will be zero, then the determinant will also be close to zero) were used. Figure 3.2 shows the comparison between all those three quantities and confirms that they all point to the same frequencies of the collective excitations.

The results of our calculations are shown in Figures 3.3-3.5. The small circle marks collective frequencies as a function of the interaction  $k_F a$ . The color marks the gap-to-density ratio  $R = \frac{S_\Delta^2}{S_\Delta^2 + S_\rho^2}$ , where  $S_\Delta = \sqrt{S_{\uparrow\downarrow}^2 + S_{\downarrow\uparrow}^2}$ ,  $S_\rho = \sqrt{S_{\uparrow\uparrow}^2 + S_{\downarrow\downarrow}^2}$

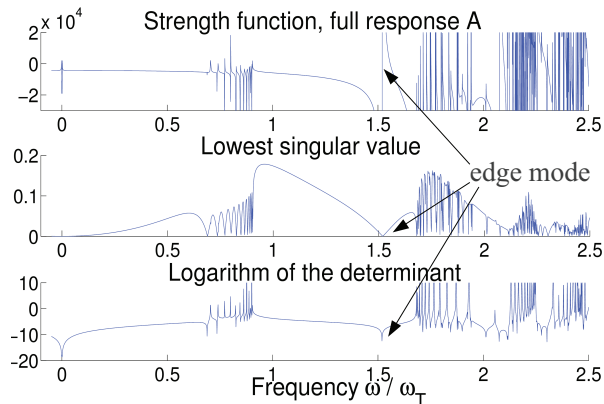


**Figure 3.2.** Comparison of three quantities: the full response, the lowest singular value and logarithm of the determinant, as the sources of the frequencies of the collective excitations. Reproduced with permission from Publication III of this thesis.

and  $S_{ij}$ ,  $i, j = \{\uparrow, \downarrow\}$  is the density response  $S_{ij}(\omega) = \int dr_1 dr_3 r_1^2 r_5^2 \mathcal{A}_{ij, L=0}(r_1, r_5, \omega)$ . This is the quantity that one can experimentally observe if the trapping potential is modulated with frequency  $\omega$ . As the density responses  $\mathcal{A}_{\uparrow\uparrow, L=0}$  and  $\mathcal{A}_{\downarrow\downarrow, L=0}$  are directly showing the change in the gap, and  $\mathcal{A}_{\uparrow\downarrow, L=0}$  and  $\mathcal{A}_{\downarrow\uparrow, L=0}$  the change in the density, they can be used as indicators of the type of the mode. The reason for introducing the gap-to-density ratio  $R$  is that for some collective excitations only the gap is changed and for some others only the density. Experimentally it is easy to detect changes which is marked in the same Figure 3.3.

The especially interesting modes are the ones of the low energy band which start from  $\omega = 0$  for interaction  $k_F a = 0$  and the frequencies of which are growing with increasing interaction and which merge with the other bands for  $k_F a \sim -0.8$ . The low energy band is explicitly marked in Figure 3.3 and is recognizable in Figures 3.4 and 3.5. The author identifies this low-energy band as a Higgs-like mode: the Higgs mode is a collective mode associated with the amplitude fluctuations of the order parameter. Here the order parameter is the superfluid pairing gap  $\Delta$  and the excitation energy of the mode in the weakly interacting limit is approximately  $2\Delta$ . The Higgs mode can be experimentally challenging to detect since it is only weakly coupled to the atom densities, as seen in the color coding of Figure 3.3. However, in Publication III it was suggested that such gap modes can be detected experimentally by ramping the interactions to the BEC side and thus mapping the pairing gap modulations into molecular density modulations.

The other prominent mode is an edge mode, marked in Figures 3.2 and 3.3. It starts from  $\omega = 2\omega_T$  for  $k_F a = 0$ , continues between  $\omega = 1.5\omega_T$  and  $\omega = 2\omega_T$  and

finally merges with the other bands at the same point where the low energy band is merging. This mode is called an edge mode as from the analysis of the mode spatial extent one can see that the gas is excited mostly near the edge. The edge mode is the strongest one (see Figure 3.2) and it is purely collective: there are no related single-particle modes as for the other modes. This mode is identified to be of the type of so-called Leggett mode, which appears when there are two bands in a superconductor, and the collective excitation corresponds to pairs moving between those two bands. Remembering from Equation 3.35 that the gap is connected with the Green's function as  $\Delta(\mathbf{r}, \mathbf{t}) = \widehat{G}_{\uparrow\downarrow}(\mathbf{r}, \mathbf{r}, t)$ , from Equation 3.63 it is possible to see that total gap is a sum of gaps for different angular momenta  $l$ :  $\Delta(\mathbf{r}, \mathbf{t}) = \Delta_{l=0}(\mathbf{r}, \mathbf{t}) + \Delta_{l=1}(\mathbf{r}, \mathbf{t}) + \dots$ . Due to the spherical symmetry,  $l$  is a good quantum number and different  $l$ -s can be considered as different channels (bands). The Leggett mode corresponds to the transition between two different bands, or two channels with the different angular momenta. Like the Higgs-like mode discussed above, also the Leggett mode is primarily a gap mode. However, the Leggett mode involves the internal structure of the total order parameter.

For the higher temperatures the appearance of second sound-type modes see in Figure 3.5. Figure 3.5 shows that the modes do not exist for zero temperature but appear for finite temperatures instead. This mode corresponds to transitions where thermal excitations are essential, as explained in Publication III.

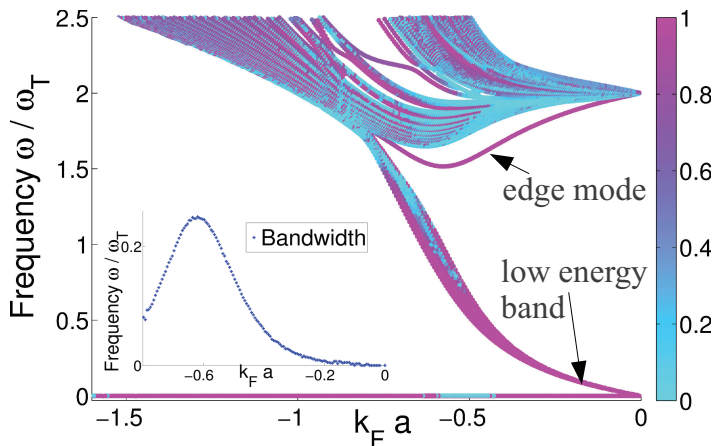


**Figure 3.3.** Collective mode frequencies as function of the interaction  $k_F a$  for  $T = 0$ . The color marks the gap-to-density ratio  $R$  (see text): blue is for  $R = 0$ , red for  $R = 1$ . Here and in the following figures  $\omega_T$  is the trapping frequency. Reproduced with permission from Publication III of this thesis.

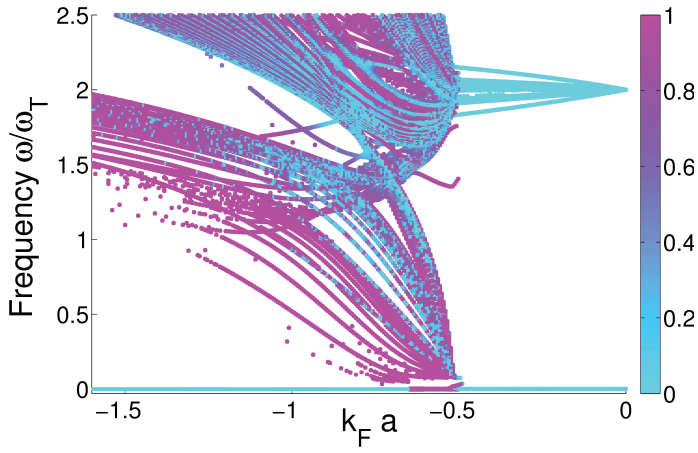


**Figure 3.4.** Collective mode frequencies as a function of the interaction  $k_F a$  for  $T = 0.2$ . The color marks the gap-to-density ratio  $R$  (see text): blue is for  $R = 0$ , red for  $R = 1$ . Reproduced with permission from Publication III of this thesis.

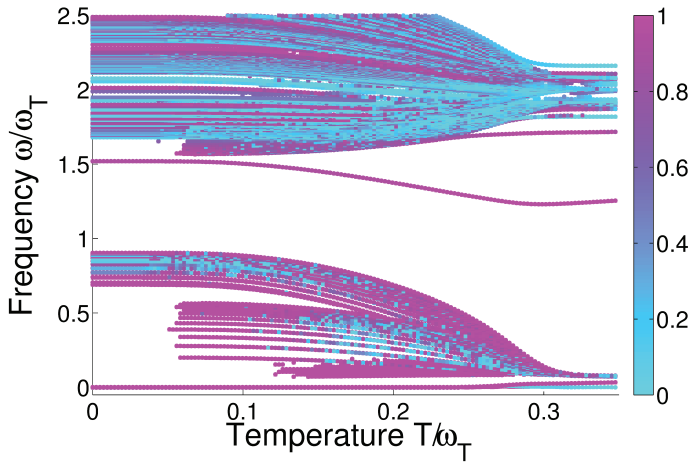


**Figure 3.5.** Collective mode frequencies as a function of the temperature  $T$  for the interaction  $k_F a = -0.56$ . The color marks the gap-to-density ratio  $R$  (see text): blue is for  $R = 0$ , red for  $R = 1$ . Reproduced with permission from Publication III of this thesis.

## 4. TEBD (Time-Evolving Block Decimation) method

The time-evolving block decimation (TEBD) algorithm [103, 104] is designed for essentially exact calculations of the evolution of a one-dimensional (1D) system at zero temperature. The algorithm is very effective, allowing the treatment of systems with low level of entanglement using moderate amount of computational resources. The TEBD algorithm is related to the famous density matrix renormalization group (DMRG) algorithm [105]: both of them rely on the description of the wave function using a product of matrices, or the matrix product state (MPS). The main difference between the two is the logic for truncating the Hilbert space, which is the trick that makes the algorithm tractable.

First in this chapter is given a general overview of DMRG and TEBD so far as they share the same general principles. The details of TEBD will be discussed later. The TEBD discussion part is based on publications by G. Vidal [103, 104] and describes the structure of the algorithm.

### 4.1 DMRG (Density Matrix Renormalization Group) method

The DMRG (Density Matrix Renormalization Group) algorithm was developed in the 90's in order to solve the problems which arise when renormalization is applied to 1D quantum systems [105, 106]. Figure 4.1 schematically shows how the DMRG method works. The system is divided into two blocks ( $B$  and  $B'$ ) and two sites between them ( $a$  and  $a'$ ). Assuming that the Hamiltonian has at most nearest neighbor interactions, one can calculate the matrix element of the local Hamiltonian  $H_{BB'aa'}$ , which treats the subsystems  $B$  and  $B'$  as two immutable entities (since the local Hamiltonian acts only on sites  $a$  and  $a'$ ). This local Hamiltonian is diagonalized and, if needed, part of the eigenstates are neglected, effectively truncating the Hilbert space to span only the most relevant states. Then new blocks  $B_{new}$  and  $B'_{new}$  are formed, where  $B_{new}$  includes the block  $B$  and the lattice site  $a$ ,  $B'_{new}$  is  $B'$  without its edge left lattice site (which

becomes  $a'_{new}$ , and  $a_{new} = a'$ . And now the above step is repeated. For each step of this algorithm the boundary between the blocks is moving one lattice site to the right. After a full sweep (when the edge traverses the whole lattice) the energy of the state is calculated. The method is iterative, so that in each sweep the answer becomes closer and closer to the true ground state energy of the system, if convergence is achieved.

Although the DMRG and TEBD algorithms have a lot in common (mainly that they both use splitting of the system into two parts and treating big chunks of the chain as one entity), they have been developed independently. DMRG has been developed by S.White [105] in 1992 and TEBD by G. Vidal [103, 104] in 2003. Both algorithms are widely used in simulations of quantum systems. Main value both in DMRG and TEBD is that both of them at each step are distinguishing the most important parts of the quantum states describing the system and leaving out the rest.

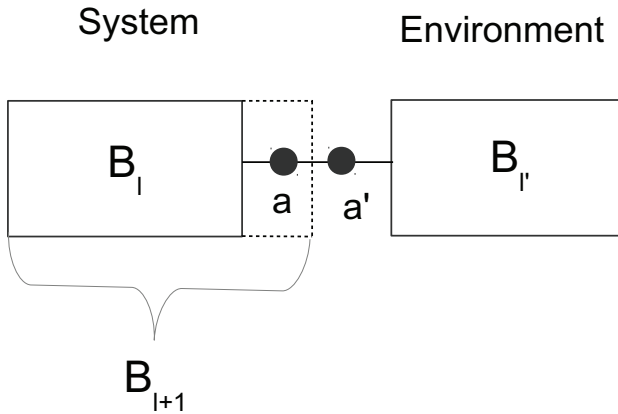


**Figure 4.1.** Schematic representation of one step in the DMRG method. The lattice (“the universe”) is split into four parts: “the system” block  $B_l$ , “the environment” block  $B_l'$  and two sites in between,  $a$  and  $a'$ . After a local operation on sites  $a$  and  $a'$ , new blocks are formed by moving the boundaries by one site to the right. The dashed line marks the new block  $B_{l+1}$ .

## 4.2 TEBD: Schmidt decomposition

TEBD [103, 104] is an algorithm for simulation of quantum 1D lattice systems. It is quite similar to DMRG, but it differs in details. One of the key points in the TEBD method is the Schmidt decomposition. The usual way of representing a

wave function is to choose a basis and determine the coefficients corresponding to each basis state. To store all the coefficients of a many-body state a lot of memory space is needed and computations become practically impossible for considerable system size. The Schmidt decomposition allows one to sort the coefficients based on their importance, and to neglect the less important ones. Of course, some information about the system is lost, but the Schmidt decomposition provides a way to do the truncation of the state in a controlled manner.

Here it is shown how the Schmidt decomposition works on a lattice (a chain of sites). The lattice has  $N$  sites, which are numbered as  $i = 1 \dots N$ . The local on-site basis states are denoted as  $|k\rangle$  where  $k = 1 \dots N_{st}$ . For instance, if we consider an ultracold Fermi gas with two spins the local basis states are  $|0\rangle$ ,  $|\uparrow\rangle$ ,  $|\downarrow\rangle$  and  $|\uparrow\downarrow\rangle$ . Here  $|0\rangle$  means an empty lattice site,  $|\uparrow\rangle$  is a lattice site containing an atom with spin up,  $|\downarrow\rangle$  with spin down and  $|\uparrow\downarrow\rangle$  means that a pair resides in the lattice site.

In general any state of the lattice can be written as

$$|\psi\rangle = \sum_{k_1, k_2, \dots, k_N} \psi_{k_1, k_2, \dots, k_N} |k_1\rangle \otimes |k_2\rangle \otimes \dots \otimes |k_N\rangle. \quad (4.1)$$

Here  $|k_i\rangle$  is the basis state corresponding to the  $i$ -th lattice site.

Equation 4.1 is a decomposition of the wave function  $|\psi\rangle$  using a set of states  $|k\rangle$  as the basis. The problem of this decomposition is that in order to identify a quantum state it requires a total of  $N_{st}^N$  coefficients  $\psi_{k_1, k_2, \dots, k_N}$ ; even for a small lattice  $N \sim 40$  this number exceeds any possible computational limits. Thus, instead of the decomposition 4.1 (which scales as  $e^N$ ), the Schmidt decomposition and the truncation procedure will be used. Schmidt decomposition and the truncation are the cornerstones of the TEBD algorithm.

To show how the Schmidt decomposition works a system which contains two subsystems: A and B, is considered. The states of the system A are marked as  $|\psi\rangle_A$  and of the system B as  $|\varphi\rangle_B$ . Any state of the total system consisting both A and B can be written as

$$|\psi\rangle = \sum_{\alpha=1 \dots N_{Shm}} \lambda_\alpha |\psi_\alpha\rangle_A |\varphi_\alpha\rangle_B, \quad (4.2)$$

where  $|\psi_\alpha\rangle_A, |\varphi_\alpha\rangle_B$  are different, mutually orthogonal, states and  $\lambda_\alpha$  is a coefficient (complex number). Here  $N_{Shm}$  is the so-called Schmidt number, it is the number of states in the decomposition 4.2 (note that it is different from  $N_{st}$ ). The decomposition of Equation 4.2 is called the Schmidt decomposition.

Figure 4.2 shows how the Schmidt decomposition is utilized for the TEBD algorithm. In the first step (first row in Figure 4.2) it is chosen that the system

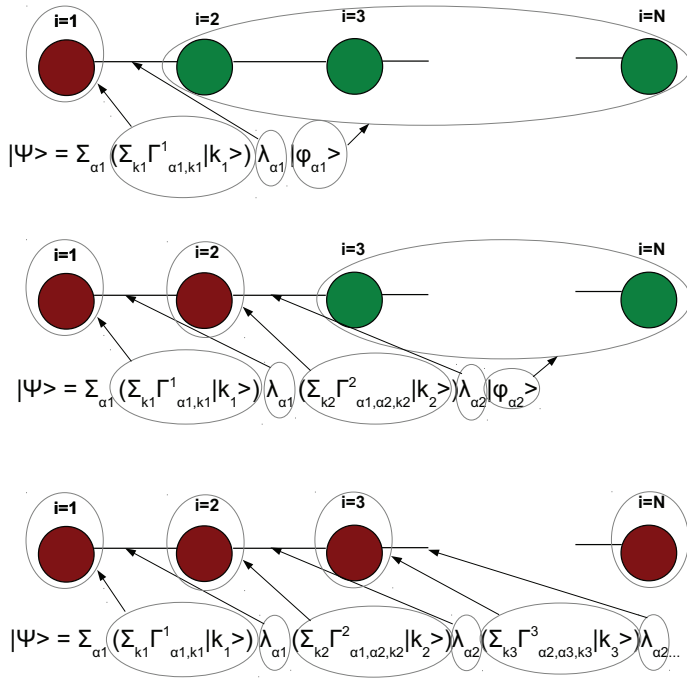


**Figure 4.2.** Schematic of the Schmidt decomposition. For every link between two neighboring lattice sites the decomposition is performed as in Equation 4.2. Instead of keeping all the coefficients  $\psi_{k_1, k_2, \dots, k_N}$  as in Equation 4.1, only  $\lambda_{\alpha_{i-1}}^{(i-1)}$  and  $\Gamma_{\alpha_{i-1} \alpha_i, k_i}^{(i)}$  from Equation 4.10 are stored.

A contains the lattice site  $i = 1$  (only one site) and the system B contains the lattice sites  $i = 2 \dots N$ . The decomposition for those two subsystems looks as the following

$$|\psi\rangle = \sum_{\alpha=1 \dots N_{Shm}} \lambda_{\alpha}^{(1)} |\psi_{\alpha}\rangle_A |\varphi_{\alpha}\rangle_B, \quad (4.3)$$

where  $\lambda_{\alpha}^{(i)}$  is a Schmidt coefficient,  $|\psi_{\alpha}\rangle_A$  is a state of the lattice site  $i = 1$  and  $|\varphi_{\alpha}\rangle_B$  is a state of the lattice sites  $i = 2 \dots N$ .

For Equation 4.3 to be correct, the following properties must be satisfied:

1) the states  $|\psi_{\alpha}\rangle_A$  as well as  $|\varphi_{\alpha}\rangle_B$  form an orthonormal basis (here  $\alpha = 1 \dots N_{Shm}$ ):

$$\langle \psi_{\alpha} | \psi_{\beta} \rangle_A = \delta_{\alpha\beta} \quad (4.4)$$

$$\langle \varphi_{\alpha} | \varphi_{\beta} \rangle_B = \delta_{\alpha\beta} \quad (4.5)$$

2) the norm of the state  $|\psi\rangle$  (of Equation 4.3) is one. Together with the previous

property it implies:

$$\sum_{\alpha=1}^{N_{Shm}} \|\lambda_{\alpha}\|^2 = 1. \quad (4.6)$$

Now one needs to recall Equation 4.3.

The basis states for our system are  $|k\rangle$  (as in Equation 4.1), thus each of the states  $|\psi_{\alpha}\rangle_A$  can be decomposed as

$$|\psi_{\alpha}\rangle_A = \sum_k \Gamma_{\alpha,k}^{(1)} |k_1\rangle \quad (4.7)$$

(here 1 in  $|k_1\rangle$  means that the lattice site  $i = 1$  is considered). Thus the following is correct

$$|\psi\rangle = \sum_{\alpha=1 \dots N_{Shm}} \sum_{k_1} \Gamma_{\alpha,k_1}^{(1)} |k_1\rangle \lambda_{\alpha}^{(1)} |\varphi_{\alpha}\rangle_B. \quad (4.8)$$

Now the Schmidt decomposition of the state  $|\varphi_{\alpha}\rangle_B$  is made, taking the site  $i = 2$  as the system A and the sites  $i = 3 \dots N$  as the system B (the second row in Figure 4.2). The same logic as earlier implies

$$|\psi\rangle = \sum_{\alpha,\beta=1 \dots N_{Shm}} \sum_{k_1,k_2} \Gamma_{\alpha,k_1}^{(1)} |k_1\rangle \lambda_{\alpha}^{(1)} \Gamma_{\alpha\beta,k_2}^{(2)} |k_2\rangle \lambda_{\beta}^{(2)} |\varphi_{\beta}\rangle_B. \quad (4.9)$$

Each link between every two neighboring sites is continued to be decomposed, from left to right (shown in Figure 4.2) and finally one obtains the following:

$$\begin{aligned} |\psi\rangle = & \sum_{\alpha_1, \alpha_2, \dots, \alpha_N=1 \dots N_{Shm}} \sum_{k_1, k_2, \dots, k_N} \Gamma_{\alpha_1, k_1}^{(1)} \lambda_{\alpha_1}^{(1)} \Gamma_{\alpha_1 \alpha_2, k_2}^{(2)} \dots \lambda_{\alpha_{i-1}}^{(i-1)} \Gamma_{\alpha_{i-1} \alpha_i, k_i}^{(i)} \\ & \dots \lambda_{\alpha_N}^{(N-1)} \Gamma_{\alpha_N, k_N}^{(N)} |k_1\rangle |k_2\rangle \dots |k_i\rangle \dots |k_N\rangle. \end{aligned} \quad (4.10)$$

Equation 4.10 is the Schmidt decomposition of the lattice wave function.

How many coefficients one needs to store in order to describe the state  $|\psi\rangle$  decomposed as in Equation 4.10? Each of the vectors  $\lambda$  has  $N_{Shm}$  coefficients, and each of matrices  $\Gamma$  has  $N_{Shm} * N_{Shm} * N_{st}$ . So the majority of the memory requirement comes from storing the  $\Gamma$  matrices and it is:

$$\sim N * N_{Shm} * N_{Shm} * N_{st}, \quad (4.11)$$

which is linearly proportional to  $N$ , but the Schmidt numbers  $N_{Shm}$  scale exponentially with  $N$  if one expresses the quantum state exactly. The key point is, however, that the Schmidt decomposition allows to truncate the state in a controlled manner, reducing  $N_{Shm}$  dramatically. This scaling is the main reason for the utility of the TEBD algorithm.

As one wins in the memory storage and speed, one loses instead in accuracy. If  $N_{Shm}$  would be such that all the states are taken into account (which means

that  $N_{Shm}$  should be around  $N_{st}^{N-1}$ , the solution would be exact. But usually it is chosen  $N_{Shm}$  much smaller (e.g. for our calculations  $N = 40$ ,  $N_{st} = 4$  and  $N_{Shm} = 100$ ) and this is where one wins in the computational resources. The key property here is that for systems with only a low level of entanglement, the required Schmidt number for a very high accuracy does not increase rapidly with the size of the system. As Vidal shows [103, 104], for quantum systems with low enough entanglement the loss of accuracy due to the truncation is small and can be controlled.

### 4.3 TEBD algorithm

After the thorough discussion of the Schmidt decomposition let us move to the TEBD algorithm itself. The time-evolution of the wave function is given by the Schrödinger equation, which for a time independent Hamiltonian  $\hat{H}$  gives

$$|\psi(t)\rangle = e^{-i\hat{H}t} |\psi(t=0)\rangle. \quad (4.12)$$

As the Equation 4.10 tells, the coefficients  $\lambda$  and  $\Gamma$  characterize the system state  $|\psi\rangle$  so they are changed during the evolution of the system. The coefficients  $\lambda_{\alpha_{i-1}}^{(i-1)}$  and  $\Gamma_{\alpha_{i-1}\alpha_i k_i}^{(i)}$  thus become:  $\lambda_{\alpha_{i-1}}^{(i-1)}(t)$ ,  $\Gamma_{\alpha_{i-1}\alpha_i k_i}^{(i)}(t)$ . The time dependence can be determined by knowing the Hamiltonian of Equation 4.12.

In case of the general Hamiltonian the calculations will be quite demanding, but it is possible to simplify them when there is a Hamiltonian of the type

$$\hat{H} = \sum \hat{H}_i + \sum \hat{H}_{i,i+1}. \quad (4.13)$$

Here  $\hat{H}_i$  means a single site term, which acts only on a single lattice site  $i$  (e.g. trap energy  $V_i n_i$ , where  $V_i$  is a trap at lattice site  $i$  and  $n_i$  is the density at the same place). Here  $\hat{H}_{i,i+1}$  describes a term which acts on two adjacent lattice sites  $i$  and  $i+1$  (e.g. the hopping term from the Hubbard Hamiltonian  $\hat{c}_{i,\uparrow}^\dagger \hat{c}_{i+1,\uparrow}$ , where  $\hat{c}_{i+1,\uparrow}$  destroys the up particle on the site  $i+1$  and  $\hat{c}_{i,\uparrow}^\dagger$  creates the up particle on the site  $i$ ). For instance, the Hubbard Hamiltonian is of such a type. In this case it is possible to calculate the evolution with affordable computational cost (the number of operations per time step will be around  $\sim N * N_{Shm} * N_{Shm} * N_{Shm}$ ). These calculations are considered in detail in the following subsection.

#### 4.3.1 Hamiltonian $\hat{H}_i$ for one lattice site

First the case in which the Hamiltonian contains only the one-site Hamiltonian is considered or  $\hat{H} = \sum_i \hat{H}_i$ . For such a case, Equation 4.10 is rewritten as

$$|\psi\rangle = \sum_{\alpha_i, \alpha_{i+1}=1}^{N_{sh}} \sum_{k_i=1}^{N_{st}} |\phi_{\alpha_{i-1}}\rangle \lambda_{\alpha_{i-1}}^{(i-1)} \Gamma_{\alpha_{i-1}\alpha_i, k_i}^{(i)} |k_i\rangle \lambda_{\alpha_i}^{(i)} |\varphi_{\alpha_i}\rangle. \quad (4.14)$$

Here  $|\phi_{\alpha_{i-1}}\rangle$  is a state which contains all lattice sites  $1..i-1$  and  $|\varphi_{\alpha_i}\rangle$  includes lattice sites  $i+1..N$ . Both of them form an orthonormal basis, as required in Equations 4.4-4.5.

The Hamiltonian can be expressed as

$$\hat{H} = H^{(1)} \otimes 1 \otimes 1 \dots + \otimes 1 \otimes H^{(1)} \otimes 1 \dots + \dots + \dots \otimes 1 \otimes 1 \otimes H^{(1)}, \quad (4.15)$$

where  $H^{(1)}$  acts on the Hilbert space of one site where basis vectors are  $|k\rangle$ . For the time-evolution the exponent of this Hamiltonian is needed, or (here  $\hbar = 1$ )

$$\hat{O} = e^{-i\sum_{i=1}^N H_i t}. \quad (4.16)$$

Different operators  $H_i$  and  $H_j$  act on the different lattice sites and hence they commute:

$$[\hat{H}_i, \hat{H}_j] = 0. \quad (4.17)$$

The time-evolution operator  $\hat{O}$  is thus just a product of the operators which act on the different lattice sites:

$$\hat{O} = \prod_{i=1}^N \hat{O}_i. \quad (4.18)$$

If  $\hat{H}$  is written as in Equation 4.15, then

$$\hat{O} = \prod_{i=1}^N \hat{O}_i = \prod_{i=1}^N e^{-i\hat{H}_i t} = e^{-i\hat{H}_1^{(1)} t} \otimes e^{-i\hat{H}_2^{(1)} t} \otimes e^{-i\hat{H}_3^{(1)} t} \otimes \dots \otimes e^{-i\hat{H}_N^{(1)} t}. \quad (4.19)$$

Here the subscript  $i$  in  $\hat{H}_i^{(1)}$  means the site that the single site operator acts on.

Let us consider separately how the operator  $\hat{O}$  works on some fixed lattice site  $i$ , or the term  $e^{-i\hat{H}_i t}$ . For the wave function Equation 4.14 is used and one obtains

$$\hat{O}_i |\psi\rangle = \sum_{\alpha_i, \alpha_{i+1}=1}^{N_{sh}} \sum_{k_i=1}^{N_{st}} |\phi_{\alpha_{i-1}}\rangle \lambda_{\alpha_{i-1}}^{(i-1)} \Gamma_{\alpha_{i-1}\alpha_i, k_i}^{(i)} e^{-i\hat{H}_i^{(1)} t} |k_i\rangle \lambda_{\alpha_i}^{(i)} |\varphi_{\alpha_i}\rangle. \quad (4.20)$$

The operator  $\hat{O}_i = e^{-i\hat{H}_i^{(1)} t}$  acts only on the lattice site  $i$  transforming the basis state  $|k_i\rangle$  as

$$e^{-i\hat{H}_i^{(1)} t} |k_i\rangle = \sum_{l_i=1}^{N_{st}} O_{k_i l_i} |l_i\rangle. \quad (4.21)$$

Thus Equation 4.20 becomes

$$\hat{O}_i |\psi\rangle = \sum_{\alpha_i, \alpha_{i+1}=1}^{N_{Shm}} \sum_{k_i, l_i=1}^{N_{St}} |\phi_{\alpha_{i-1}}\rangle \lambda_{\alpha_{i-1}}^{(i-1)} \Gamma_{\alpha_{i-1}\alpha_i, k_i}^{(i)} O_{k_i l_i} |l_i\rangle \lambda_{\alpha_i}^{(i)} |\varphi_{\alpha_i}\rangle \quad (4.22)$$

or

$$\hat{O}_i |\psi\rangle = \sum_{\alpha_i, \alpha_{i+1}=1}^{N_{Shm}} \sum_{l_i=1}^{N_{St}} |\phi_{\alpha_{i-1}}\rangle \lambda_{\alpha_{i-1}}^{(i-1)} \Gamma_{\alpha_{i-1}\alpha_i, l_i}^{(i)} |l_i\rangle \lambda_{\alpha_i}^{(i)} |\varphi_{\alpha_i}\rangle, \quad (4.23)$$

where

$$\Gamma_{\alpha_{i-1}\alpha_i, l_i}^{(i)} = \sum_{k_i=1}^{N_{St}} \Gamma_{\alpha_{i-1}\alpha_i, k_i}^{(i)} O_{k_i l_i}. \quad (4.24)$$

This is the same equation as Equation 4.14, just with  $\Gamma'$  instead of  $\Gamma$ . Thus one comes to the very important conclusion: the one-site operator  $\hat{H}_i^{(1)}$ , by acting on the lattice site  $i$ , changes only the corresponding coefficient  $\Gamma_{\alpha_{i-1}\alpha_i, k_i}^{(i)}$  according to Equation 4.24.

### 4.3.2 Hamiltonian $\hat{H}_{i,i+1}$ for two adjacent lattice sites

The next step is to calculate how do  $\lambda_{\alpha_{i-1}}^{(i-1)}$  and  $\Gamma_{\alpha_{i-1}\alpha_i, k_i}^{(i)}$  change in case of a Hamiltonian which acts on two neighboring sites.

First, the operator  $\hat{O}_{i,i+1}$ , which acts only on two lattice sites  $i$  and  $i+1$ , is considered. How the local time-evolution operator  $\hat{O}_{i,i+1}$  depends on the Hamiltonian  $\hat{H}_{i,i+1}$ , will be considered in the next Subsection 4.3.3.

Now one has to separate two lattice sites from the wave function or rewrite  $|\psi\rangle$  as

$$|\psi\rangle = \sum_{\alpha_{i-1}, \alpha_i, \alpha_{i+1}=1}^{N_{Shm}} \sum_{k_i, k_{i+1}=1}^{N_{St}} |\phi_{\alpha_{i-1}}\rangle \lambda_{\alpha_{i-1}}^{(i-1)} \Gamma_{\alpha_{i-1}\alpha_i, k_i}^{(i)} |k_i\rangle \lambda_{\alpha_i}^{(i)} \Gamma_{\alpha_i \alpha_{i+1}, k_{i+1}}^{(i+1)} |k_{i+1}\rangle \lambda_{\alpha_{i+1}}^{(i+1)} |\varphi_{\alpha_{i+1}}\rangle. \quad (4.25)$$

Here  $\hat{O}_{i,i+1}$  acts as:

$$\hat{O}_{i,i+1} |k_i\rangle |k_{i+1}\rangle = \sum_{l_i, l_{i+1}=1}^{N_{St}} O_{k_i k_{i+1}, l_i l_{i+1}} |l_i\rangle |l_{i+1}\rangle. \quad (4.26)$$

Then Equation 4.26 together with Equation 4.25 implies the following:

$$\hat{O}_{i,i+1} |\psi\rangle = \sum_{\alpha_{i-1}, \alpha_i, \alpha_{i+1}=1}^{N_{Shm}} \sum_{k_i, k_{i+1}, l_i, l_{i+1}=1}^{N_{St}} |\phi_{\alpha_{i-1}}\rangle \lambda_{\alpha_{i-1}}^{(i-1)} \Gamma_{\alpha_{i-1}\alpha_i, k_i}^{(i)} \lambda_{\alpha_i}^{(i)} \Gamma_{\alpha_i \alpha_{i+1}, k_{i+1}}^{(i+1)} O_{k_i k_{i+1}, l_i l_{i+1}} |l_i\rangle |l_{i+1}\rangle |\varphi_{\alpha_{i+1}}\rangle. \quad (4.27)$$

Now the two coefficients  $\Gamma_{\alpha_{i-1}\alpha_i, k_i}^{(i)}$  and  $\Gamma_{\alpha_i \alpha_{i+1}, k_{i+1}}^{(i+1)}$  are involved, as well as the coefficient  $\lambda_{\alpha_i}^{(i)}$  between them. So all these three coefficients should be changed simultaneously to  $\Gamma_{\alpha_{i-1}\alpha_i, l_i}^{(i)}$ ,  $\Gamma_{\alpha_i \alpha_{i+1}, l_{i+1}}^{(i+1)}$  and  $\lambda_{\alpha_i}^{(i)}$ , such that

$$\Gamma_{\alpha_{i-1}\alpha_i,l_i}^{(i)} \lambda_{\alpha_i}^{(i)} \Gamma_{\alpha_i\alpha_{i+1},l_{i+1}}^{(i+1)} = \sum_{k_i,k_{i+1}=1}^{N_{st}} \Gamma_{\alpha_{i-1}\alpha_i,k_i}^{(i)} \lambda_{\alpha_i}^{(i)} \Gamma_{\alpha_i\alpha_{i+1},k_{i+1}}^{(i+1)} O_{k_i k_{i+1}, l_i, l_{i+1}}. \quad (4.28)$$

The additional constraints are that

$$\sum_{\alpha_i=1}^{N_{Shm}} \left| \lambda_{\alpha_i}^{(i)} \right|^2 = 1 \quad (4.29)$$

and

$$\sum_{\alpha_{i-1}=1}^{N_{Shm}} \Gamma_{\alpha_{i-1}\alpha_i,l_i}^{(j)} \Gamma_{\alpha_{i-1}\alpha'_i,l'_i}^{(j)} = \delta_{\alpha_i,\alpha'_i} \delta_{l_i,l'_i} \quad (4.30)$$

$$\sum_{\alpha_i=1}^{N_{Shm}} \Gamma_{\alpha'_{i-1}\alpha_i,l_i}^{(j)} \Gamma_{\alpha'_{i-1}\alpha_i,l'_i}^{(j)} = \delta_{\alpha_{i-1},\alpha'_{i-1}} \delta_{l_i,l'_i} \quad (4.31)$$

for  $j = i$  and  $j = i + 1$ . These constraints come from Equations 4.4-4.6. So for solving Equation 4.28 one has to find the right-hand side of the equation, and after that to find  $\Gamma_{\alpha_{i-1}\alpha_i,l_i}^{(i)}$ ,  $\Gamma_{\alpha_i\alpha_{i+1},l_{i+1}}^{(i+1)}$  and  $\lambda_{\alpha_i}^{(i)}$  which additionally satisfy the constraints 4.29-4.31. Solving the Equation 4.28 is equivalent for the Schmidt decomposition, as described in Section 4.2.

For the Hamiltonian acting on three adjacent sites, the algorithm is similar: separate three sites, e.g.  $i - 1, i, i + 1$ , find out how the three-site Hamiltonian acts on them, find out the new coefficients  $\lambda$  and  $\Gamma$ . But the amount of required computational resources will be higher. For the one-site operator one needs to change only  $\Gamma^{(i)}$ , for the two-site operator  $\Gamma^{(i)}$ ,  $\Gamma^{(i+1)}$  and  $\lambda^{(i)}$  are involved, but for a three site operator it is needed to change five coefficients:  $\Gamma^{(i-1)}$ ,  $\Gamma^{(i)}$ ,  $\Gamma^{(i+1)}$ ,  $\lambda^{(i)}$ ,  $\lambda^{(i-1)}$ . This requires a lot of computational power. In practice three-site Hamiltonian can be the Hubbard Hamiltonian with the next-nearest neighbor interaction, e.g. when hopping is possible not only between the adjacent site but also between the second neighbors, which are on the lattice sites  $i - 1$  and  $i + 1$ .

### 4.3.3 Time-evolution

For TEBD calculations in this thesis the Hubbard Hamiltonian was used:

$$\begin{aligned} \hat{H} &= -J \sum_{i,s=\{\uparrow\downarrow\}} \left( \hat{c}_{i,s}^\dagger \hat{c}_{i+1,s} + \hat{c}_{i+1,s}^\dagger \hat{c}_{i,s} \right) + \frac{U}{2} \sum_i \hat{n}_{i,\uparrow} \hat{n}_{i,\downarrow} + \sum_{i,s} \epsilon_{i,s} \hat{n}_{i,s} \\ &= \sum_i \hat{H}_{i,i+1} + \sum_i \hat{H}_i, \end{aligned} \quad (4.32)$$

where  $\hat{H}_{i,i+1}$  means the hopping part (two-site Hamiltonian) and  $\hat{H}_i$  the trap energy and the pairing energy (one-site Hamiltonian).

For calculating the time-evolution of the wave function from the moment of time  $t = 0$  to the moment of time  $t$ , the exponent  $e^{-i\hat{H}t}$  is needed. Let us divide the time-evolution into small steps  $\delta t$ , and calculate  $e^{-i\hat{H}\delta t} * e^{-i\hat{H}\delta t} * e^{-i\hat{H}\delta t} * \dots * e^{-i\hat{H}\delta t}$ , where the exponents are multiplied  $\frac{t}{\delta t}$  times. It is the same operator  $\left(e^{-i\hat{H}\delta t}\right)^{\frac{t}{\delta t}} = e^{-i\hat{H}t}$ , but now, for calculating  $e^{-i\hat{H}\delta t}$  one can use the Suzuki-Trotter expansion

$$e^{-i\hat{H}\delta t} = e^{-i\sum_i(\hat{H}_{i,i+1}+\hat{H}_i)\delta t} \approx \prod_i e^{-i(\hat{H}_{i,i+1}+\hat{H}_i)\delta t} \quad (4.33)$$

and operate on the lattice site by site, by first calculating  $e^{-i(\hat{H}_{1,2}+\hat{H}_1)\delta t}$ , then  $e^{-i(\hat{H}_{2,3}+\hat{H}_2)\delta t}$  and so on. Completing one sweep (from  $e^{-i(\hat{H}_{1,2}+\hat{H}_1)\delta t}$  to  $e^{-i(\hat{H}_{N-1,N}+\hat{H}_N)\delta t}$  and  $e^{-i\hat{H}_N\delta t}$ ) is equivalent to the full time-evolution for the time  $\delta t$ ; to reach the moment of time  $t$  one has to make  $\frac{t}{\delta t}$  of such sweeps. If  $\delta t$  is sufficiently small, then Equation 4.33 is correct with high enough accuracy.

Returning to the comment about the connection between  $\hat{H}_{i,i+1}$  and  $\hat{O}_{i,i+1}$  (mentioned in Subsection 4.3.2), Equation 4.33 shows indeed that the time-evolution operator can be expressed in terms of local operators:

$$\hat{O}_{i,i+1} = e^{-i(\hat{H}_{i,i+1}+\hat{H}_i)\delta t}. \quad (4.34)$$

If our model contained only single site Hamiltonians the methods from Subsection 4.3.1 could be used; this would simplify the calculations a lot. But as the Hubbard model already contains the hopping between neighboring sites, one needs to solve Equation 4.28.

#### 4.3.4 Ground state

Although the above description of the TEBD algorithm involved the real time evolution, it can also be used for finding a ground state and for calculating different observables, especially the ground state energy. For this the imaginary time-evolution (in which instead of the real time  $t$ , the evolution in imaginary time  $-it$ ) is considered:

$$|\psi_{GS}\rangle = \lim_{t \rightarrow \infty} \frac{e^{-i\hat{H}(-it)} |\psi_{In}\rangle}{\|e^{-i\hat{H}(-it)} |\psi_{In}\rangle\|} = \lim_{t \rightarrow \infty} \frac{e^{-\hat{H}t} |\psi_{In}\rangle}{\|e^{-\hat{H}t} |\psi_{In}\rangle\|}, \quad (4.35)$$

where  $\|\dots\|$  means norm of the state,  $|\psi_{GS}\rangle$  is the ground state and  $|\psi_{In}\rangle$  is the initial state, from which the calculations are started. If  $\langle \psi_{GS} | \psi_{In} \rangle \neq 0$  then no matter from which initial state one starts, he always finishes with the ground state (the state with the smallest energy).

## 4.4 Key results

Using the TEBD method, the author has done the calculations for the publications I and IV.

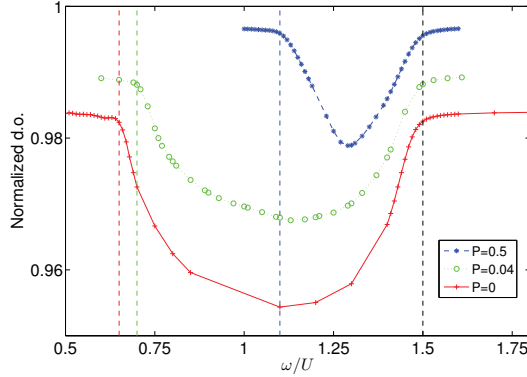


**Figure 4.3.** Double occupancy for a fixed moment of time  $t = 10$ . Different colors represent the different polarizations  $P$ . Reproduced with permission from Publication I of this thesis.

The publication I studied the Fulde-Ferrell-Larkin-Ovchinnikov (FFLO) state in a 1D lattice with ultracold Fermions. The system was excited with the help of lattice modulation, that is, the hopping energy was  $J(t) = J + \delta J \cos \omega t$  with the modulation frequency  $\omega$ . With the help of the TEBD algorithm the author was calculating the time-evolution when the modulation is applied. As a result, for certain frequencies the double occupancy, that is, the number of sites with both spin up and spin down atoms, does not change, but for certain others it starts to decrease. Apparently, this means that the range of the frequencies which leads to the change in the double occupancy corresponds to excitations that break the doublons. The double occupancy for a fixed moment of time  $t = 10$  is shown in Figure 4.3 for a few different polarizations. Since the FFLO state which occurs for density-imbalanced systems was of interest, different polarizations  $P = \frac{N_{\uparrow} - N_{\downarrow}}{N_{\uparrow} + N_{\downarrow}}$  were considered. It can be seen that for each polarization there is a range of resonant frequencies with the same upper boundary  $\omega \sim 1.5U$  for all polarizations but a different lower boundary. The important finding is that the bandwidth satisfies  $\Delta\omega = 4J(1 + \cos q)$ , where  $q$  is the FFLO wave vector as calculated from the ground-state distribution of the momentum. Thus the bandwidth directly reveals the existence of the FFLO state via the relation to  $q$ . The double occupancy is straightforward to detect experimentally, thus the author suggests this method for experimental probing of the FFLO state.

The publication IV studied a polaron in a 1D lattice in a situation when there

is only one atom of the minority component. The publication studied properties of the polaron in a trap. The author compared the essentially exact results given by TEBD to a variational method for describing the polaron, testing how well does the variational ansatz work in 1D. It was found that the energies are very well reproduced, while densities not equally well. Also the limits of validity of the lowest band Hubbard model and the tight binding approximation were investigated. It was found that especially the physics related to the concept of contact describing behavior at short length scales is not well captured by the lowest band model.

## 5. Conclusions

In this thesis the author numerically simulated certain configurations of systems of ultracold Fermi gases and searched for the frequencies of the collective excitations for those systems. Additionally, the author numerically calculated the energy of the polaron in a 1D lattice.

The thesis consists of two parts, the main difference being the applied method. In the first part (publications II and III) the main instruments are density response theory and the Bogolyubov-de-Gennes theory, which are used for studying a gas in a three-dimensional (3D) spherically symmetric trap. In the second part (publications I and IV) the main method is time-evolving block decimation (TEBD) algorithm and a one-dimensional (1D) lattice system is studied. Although these two methods are different and they are applied to essentially different configurations (a lattice and a harmonic trap), they can both be used for probing the collective excitations of the system.

The density response theory is based on the calculation of the linear response of the density to the external perturbation. If one, for example, modulates the system with a fixed frequency, it starts to resonate only for certain frequencies which are exactly those of the collective excitations of the system. One can calculate for which frequencies the system is resonating by determining the single-particle Green's functions and then by calculating the density response function with the random phase approximation. Peaks in the density response function (increased response of the system) point out the frequencies of collective excitations. Thus the author was able to analyze how collective excitations depend on the interactions in the system and find the detailed description of the collective modes. This was done in publication II for zero temperature and in publication III for finite temperatures, for the system of the two-component Fermi gas confined in a harmonic potential.

The TEBD algorithm is designed to simulate one dimensional quantum lattice systems which have low enough entanglement. In such cases calculations

can be speeded up while no essential information is lost. The author used the TEBD algorithm in publications I and IV. In publication I an imbalanced Fermi gas for different spin-density polarizations was simulated and the range of collective frequencies was found. In publication IV the polaron case (an imbalanced gas with only one atom of the other spin) was considered and the energy of the polaron is determined. In both cases, the use of the TEBD algorithm allows essentially exact studies in far bigger system sizes (close to the experimental reality) than would be possible by exact diagonalization.

This thesis increases understanding of the nature of processes in ultracold Fermi gases, especially of collective excitations. Publication II gives a detailed description of collective modes for zero temperature. Particularly important results are presented in publication III, in which a detailed description of collective excitations of a trapped two-component Fermi gas at finite temperature is given. The author has identified several collective modes, such as a low energy Higgs-like mode, a second sound-like mode as well as a strong edge mode analogous to the Leggett-mode. Publication I suggests a novel way of identifying the Fulde-Ferrell-Larkin-Ovchinnikov (FFLO) state in experiments with the help of lattice depth modulation spectroscopy. Publication IV compares a variational ansatz and the TEBD simulations in description of a polaron.

In the future, publications II and III could be extended to simulation of the gas in a non-symmetrical trap. In experiments, non-symmetric traps are typically used. Publication IV can be extended by introducing a disorder potential, mass imbalance and long-range interactions. The spectral width as a signature of the FFLO state as identified in publication I indicates that similar signatures could be found related to other interesting many-body states, such as those produced by long-range interactions.

# Bibliography

- [1] M. R. Andrews, C. G. Townsend, H.-J. Miesner, D. S. Durfee, D. M. Kurn, and W. Ketterle. Observation of interference between two Bose condensates. *Science*, 275:637, 1997.
- [2] I. Bloch, T.W. Hänsch, and T. Esslinger. Measurement of the spatial coherence of a trapped Bose gas at the phase transition. *Nature*, 403:166, 2000.
- [3] K.W. Madison, F. Chevy, W. Wohlleben, and J. Dalibard. Vortex formation in a stirred Bose-Einstein condensate. *Phys. Rev. Lett.*, 84:806, 2000.
- [4] J.R. Abo-Shaeer, C. Raman, and W. Ketterle. Formation and decay of vortex lattices in Bose-Einstein condensates at finite temperatures. *Science*, 292:476, 2001.
- [5] M. W. Zwierlein, J. R. Abo-Shaeer, A. Schirotzek, C. H. Schunck, and W. Ketterle. Vortices and superfluidity in a strongly interacting Fermi gas. *Nature*, 435:1047–1051, 2005.
- [6] S.N. Bose. Plancks Gesetz und Lichtquantenhypothese. *Z.Phys*, 26:178, 1924.
- [7] A. Einstein. Quantentheorie des einatomigen idealen Gases: Zweite Abhandlung. *Sitzungber. Preuss. Akad. Wiss.*, 3, 1925.
- [8] K.B. Davis, M.-O. Mewes, M.R. Andrews, N.J. van Druten, D.S. Durfee, D.M. Kurn, and W. Ketterle. Bose-Einstein condensation in a gas of sodium atoms. *Phys. Rev. Lett.*, 75:3969, 1995.
- [9] M.H. Anderson, J.R. Ensher, M.R. Matthews, C.E. Wieman, and E.A. Cornell. Observation of Bose-Einstein condensation in a dilute atomic vapor. *Science*, 269:198, 1995.
- [10] J. Klaers, J. Schmitt, F. Vewinger, and M. Weitz. Bose-Einstein condensation of photons in an optical microcavity. *Nature*, 468:545–548, 2010.
- [11] S. O. Demokritov, V. E. Demidov, O. Dzyapko, G. A. Melkov, A. A. Serga, B. Hillebrands, and A. N. Slavin. Bose-Einstein condensation of quasi-equilibrium magnons at room temperature under pumping. *Nature*, 443:430–433, 2006.
- [12] J. Kasprzak, M. Richard, S. Kundermann, A. Baas, P. Jeambrun, J. M. J. Keeling, F. M. Marchetti, M. H. Szymancuteska, R. Andre, J. L. Staehli, V. Savona, P. B. Littlewood, B. Deveaud, and Le Si Dang. Bose-Einstein condensation of exciton polaritons. *Nature*, 443:409–414, 2006.

- [13] M. Greiner, C. A. Regal, and D. S. Jin. Emergence of a molecular Bose-Einstein condensate from a Fermi gas. *Nature*, 426:537, 2003.
- [14] S. Jochim, M. Bartenstein, A. Altmeyer, G. Hendl, S. Riedl, C. Chin, J. Hecker Denschlag, and R. Grimm. Bose-Einstein condensation of molecules. *Science*, 302:2101, 2003.
- [15] M.W. Zwierlein, C.A. Stan, C.H. Schunck, S.M.F. Raupach, S. Gupta, Z. Hadzibabic, and W. Ketterle. Observation of Bose-Einstein condensation of molecules. *Phys.Rev.Lett.*, 91:250401, 2003.
- [16] H.F. Hess. Evaporative cooling of magnetically trapped and compressed spin-polarized hydrogen. *Phys. Rev. B*, 34:3476, 1986.
- [17] W. Ketterle and N.J. Van Druten. Evaporative cooling of trapped atoms. *Adv. At. Mol. Opt. Phys.*, 37:181, 1996.
- [18] M. Hammes, D. Rychtarik, V. Druzhinina, U. Moslener, I. Manek-Höninger, and R. Grimm. Optical and evaporative cooling of cesium atoms in the gravito-optical surface trap. *J. Mod. Opt.*, 47:2755, 2000.
- [19] C.J. Pethik and H. Smith. Bose-Einstein condensation in dilute gases. *CUP, Cambridge*, 2001.
- [20] M. Mudrich, S. Kraft, K. Singer, R. Grimm, A. Mosk, and M. Weidemüller. Sympathetic cooling with two atomic species in an optical trap. *Phys. Rev. Lett.*, 88:253001, 2002.
- [21] L. Simon and W. T. Strunz. Bose gas in a single-beam optical dipole trap. *Phys. Rev. A*, 81:063620, 2010.
- [22] U. Fano. Effects of configuration interaction on intensities and phase shifts. *Phys. Rev.*, 124:1866, 1961.
- [23] H. Feshbach. A unified theory of nuclear reactions. *Ann. Phys. (N.Y.)*, 19:287, 1962.
- [24] S. Inouye, M.R. Andrews, J. Stenger, H.J. Miesner, D.M. Stamper-Kurn, and W. Ketterle. Observation of Feshbach resonances in a Bose-Einstein condensates. *Nature*, 392:151, 1998.
- [25] Ph. Courteille, R. S. Freeland, D. J. Heinzen, F. A. van Abeelen, and B. J. Verhaar. Observation of a Feshbach resonance in cold atom scattering. *Phys. Rev. Lett.*, 81:69, 1998.
- [26] E. Timmermans, P. Tommasini, M. Hussein, and A. Kerman. Feshbach resonances in atomic Bose-Einstein condensates. *Phys. Rev.*, 315:199, 1999.
- [27] C. Chin, R. Grimm, P. Julienne, and E. Tiesinga. Feshbach resonances in ultracold gases. *Rep. Prog. Phys.*, 73:076501, 2010.
- [28] M. Greiner, O. Mandel, T. Esslinger, T.W. Hänsch, and I. Bloch. Quantum phase transition from a superfluid to a Mott insulator in a gas of ultracold atoms. *Nature*, 415:39, 2002.
- [29] D.S. Petrov, D.M. Gangardt, and G.V. Shlyapnikov. Low-dimensional trapped gases. *J. Phys. IV*, 116:3, 2004.

- [30] J. K. Chin, D. E. Miller, Y. Liu, C. Stan, W. Setiawan, C. Sanner, K. Xu, and W. Ketterle. Evidence for superfluidity of ultracold Fermions in an optical lattice. *Nature*, 443:961, 2006.
- [31] O. Morsch and M. Oberthaler. Dynamics of Bose-Einstein condensates in optical lattices. *Rev. Mod. Phys.*, 78:179, 2006.
- [32] I. Bloch, J. Dalibard, and W. Zwerger. Many-body physics with ultracold gases. *Rev. Mod. Phys.*, 80:885, 2008.
- [33] I. Bloch, J. Dalibard, and S. Nascimbene. Quantum simulations with ultracold quantum gases. *Nature Physics*, 8:267, 2012.
- [34] M. Muller, S. Diehl, G. Pupillo, and P. Zoller. Engineered open systems and quantum simulations with atoms and ions. *Advances in Atomic, Molecular, and Optical Physics*, 61:1, 2012.
- [35] S. Trotzky, Y-A. Chen, A. Flesch, I. P. McCulloch, U. Schollwöck, J. Eisert, and I. Bloch. Probing the relaxation towards equilibrium in an isolated strongly correlated one-dimensional Bose gas. *Nature Physics*, 8:325, 2012.
- [36] U. Bissbort, D. Cocks, A. Negretti, Z. Idziaszek, T. Calarco, F. Schmidt-Kaler, W. Hofstetter, and R. Gerritsma. Emulating solid-state physics with a hybrid system of ultracold ions and atoms. *Phys. Rev. Lett.*, 111:080501, 2013.
- [37] T. Akatsuka, M. Takamoto, and H. Katori. Optical lattice clocks with non-interacting bosons and fermions. *Nature Physics*, 4:954, 2008.
- [38] N. Poli, F.-Y. Wang, M. G. Tarallo, A. Alberti, M. Prevedelli, and G. M. Tino. Precision measurement of gravity with cold atoms in an optical lattice and comparison with a classical gravimeter. *Phys. Rev. Lett.*, 106:038501, 2011.
- [39] J. Kinast, S. L. Hemmer, M. E. Gehm, A. Turlapov, and J. E. Thomas. Evidence for superfluidity in a resonantly interacting Fermi gas. *Phys. Rev. Lett.*, 92:150402, 2004.
- [40] M. Bartenstein, A. Altmeyer, S. Riedl, S. Jochim, C. Chin, J.H. Denschlag, and R. Grimm. Collective excitations of a degenerate gas at the BEC-BCS crossover. *Phys. Rev. Lett.*, 92:20, 2004.
- [41] S. Giorgini, L. P. Pitaevskii, and S. Stringari. Theory of ultracold atomic Fermi gases. *Rev. Mod. Phys.*, 80:1215, 2008.
- [42] G. M. Bruun. Collective modes of trapped Fermi gases in the normal phase. *Phys. Rev. A*, 63:043408, 2001.
- [43] Y. Ohashi and A. Griffin. Superfluidity and collective modes in a uniform gas of Fermi atoms with a Feshbach resonance. *Phys. Rev. A*, 67:063612, 2003.
- [44] M. Grasso, E. Khan, and M. Urban. Temperature dependence and finite-size effects in collective modes of superfluid-trapped Fermi gases. *Phys. Rev. A*, 72:043617, 2005.
- [45] M. W. Zwierlein, A. Schirotzek, C.H. Schunck, , and W. Ketterle. Fermionic superfluidity with imbalanced spin populations. *Science*, 311:492–496, 2006.
- [46] G. B. Partridge, W. Li, R. I. Kamar, Y. Liao, and R. G. Hulet. Pairing and phase separation in a polarized Fermi gas. *Science*, 311:503–505, 2006.

- [47] Y. Liao, A. S. Rittner, T. Paprotta, W. Li, G. B. Partridge, R. G. Hulet, S. K. Baur, and E. J. Mueller. Spin-imbalance in a one-dimensional Fermi gas. *Nature*, 467:567–569, 2010.
- [48] A. Schirotzek, A. Sommer C.-H. Wu, , and M. W. Zwierlein. Observation of Fermi polarons in a tunable Fermi liquid of ultracold atoms. *Phys. Rev. Lett.*, 102:230402, 2009.
- [49] S. Nascimbene, N. Navon, K.J. Jiang, L. Tarruell, M. Teichmann, J. McKeever, F. Chevy, and C. Salomon. Collective oscillations of an imbalanced Fermi gas: axial compression modes and polaron effective mass. *Phys. Rev. Lett.*, 103:170402, 2009.
- [50] C. Kohstall, M. Zaccanti, M. Jag, A. Trenkwalder, P. Massignan, G. M. Bruun, F. Schreck, and R. Grimm. Metastability and coherence of repulsive polarons in a strongly interacting Fermi mixture. *Nature*, 485:615–618, 2012.
- [51] K. Huang and C. N. Yang. Quantum-mechanical many-body problem with hard-sphere interaction. *Phys. Rev.*, 105:767, 1957.
- [52] G. F. Gribakin and V. V. Flambaum. Calculation of the scattering length in atomic collisions using the semiclassical approximation. *Phys. Rev. A*, 48:546, 1993.
- [53] V.V. Flambaum, G.F. Gribakin, and C. Harabati. Analytical calculation of cold atom scattering. *Phys. Rev. A*, 59:1998, 1999.
- [54] T. Loftus, C. A. Regal, C. Ticknor, J. L. Bohn, and D. S. Jin. Resonant control of elastic collisions in an optically trapped Fermi gas of atoms. *Phys. Rev. Lett.*, 88:173201, 2002.
- [55] K. M. O’Hara, S. L. Hemmer, M. E. Gehm, S. R. Granade, and J. E. Thomas. Observation of a strongly interacting degenerate Fermi gas of atoms. *Science*, 298:2179, 2002.
- [56] K. E. Strecker, G. B. Partridge, and R. G. Hulet. Conversion of an atomic Fermi gas to a long-lived molecular Bose gas. *Phys. Rev. Lett.*, 91:080406, 2003.
- [57] G. M. Bruun and C. J. Pethick. Effective theory of Feshbach resonances and many-body properties of Fermi gases. *Phys. Rev. Lett.*, 92:140404, 2004.
- [58] G. B. Partridge, K. E. Strecker, R. I. Kamar, M. W. Jack, and R. G. Hulet. Molecular probe of pairing in the BEC-BCS crossover. *Phys. Rev. Lett.*, 95:020404, 2005.
- [59] A.L. Fetter and J.D. Walecka. Quantum theory of many-particle systems. *Dover publications, inc*, 2003.
- [60] R.Grimm, M. Weidemuller, and Y. B. Ovchinnikov. Optical dipole traps for neutral atoms. *Adv. At. Mol. Opt. Phys*, 42:95, 2000.
- [61] D. Jaksch and P. Zoller. The cold atom Hubbard toolbox. *Ann. Phys. (N.Y.)*, 315:52, 2005.
- [62] J. Hubbard. Electron correlations in narrow energy bands. *Proceedings of the Royal Society of London*, 1963.

- [63] E. Lieb. The Hubbard model: Some rigorous results and open problems. *XI Int. Cong. MP*, page 392, 1995.
- [64] H. Tasaki. The Hubbard model - an introduction and selected rigorous results. *Journal of Physics: Condensed Matter*, 10:4353, 1998.
- [65] E. H. Lieb and F.Y. Wu. The one-dimensional Hubbard model: a reminiscence. *Physica A*, 321:1, 2002.
- [66] L. Cooper. Bound electron pairs in a degenerate Fermi gas. *Phys. Rev.*, 104:1189, 1956.
- [67] G. Mahan. Many-particle physics. *Kluwer Academic/Plenum Publishers*, 2000.
- [68] J. Bardeen, L. N. Cooper, and J. R. Schrieffer. Theory of superconductivity. *Phys. Rev.*, 108:1175, 1957.
- [69] E. M. Lifshitz and L.P. Pitaevskii. Statistical physics (part 2). 1980.
- [70] F. Chevy and C. Mora. Ultracold polarized Fermi gases. *Reports on Progress in Physics*, 73:112401, 2010.
- [71] K. B. Gubbels and H. T. C. Stoof. Imbalanced Fermi gases at unitarity. *arXiv:1205.0568*, 2012.
- [72] F. Chevy. Universal phase diagram of a strongly interacting Fermi gas with unbalanced spin populations. *Phys. Rev. A*, 74:063628, 2006.
- [73] R. Combescot, A. Recati, C. Lobo, and F. Chevy. Normal state of highly polarized Fermi gases: Simple many-body approaches. *Phys. Rev. Lett.*, 98:180402, 2007.
- [74] A. Schirotzek, C.-H. Wu, A. Sommer, and M. Zwierlein. Observation of Fermi polarons in a tunable Fermi liquid of ultracold atoms. *Phys. Rev. Lett.*, 102:230402, 2009.
- [75] S. Giraud and R. Combescot. Highly polarized Fermi gases: One-dimensional case. *Phys. Rev. A*, 79:043615, 2009.
- [76] M.J. Leskinen, O.H. Nummi, F. Massel, and P. Törmä. Fermi-polaron-like effects in a one-dimensional (1D) optical lattice. *New Journal of Physics*, 12:073044, 2010.
- [77] P. Massignan and G. M. Bruun. Repulsive polarons and itinerant ferromagnetism in strongly polarized Fermi gases. *The European Physical Journal D*, 65:83–89, 2011.
- [78] G. M. Bruun and P. Massignan. Decay of polarons and molecules in a strongly polarized Fermi gas. *Phys. Rev. Lett.*, 105:105, 2010.
- [79] Sascha Zöllner, G. M. Bruun, and C. J. Pethick. Polarons and molecules in a two-dimensional Fermi gas. *Phys. Rev. A*, 83:021603, 2011.
- [80] P. Fulde and R. A. Ferrell. Superconductivity in a strong spin-exchange field. *Phys. Rev.*, 135:A550, 1964.
- [81] A. Larkin and Yu. Ovchinnikov. Inhomogeneous state of superconductors. *Sov. Phys. JETP*, 20:762, 1965.
- [82] G. Sarma. *J. Phys. Chem. Solids*, 24:1029, 1963.

- [83] A. Sedrakian, J. Mur-Petit, A. Polls, and H. Muther. Pairing in a two-component ultracold Fermi gas: phases with broken-space symmetries. *Phys. Rev. A*, 72:013613, 2005.
- [84] R. Combescot and C. Mora. The low-temperature Fulde-Ferrell-Larkin-Ovchinnikov phases in 3 dimensions. *Europhys. Lett.*, 68:79, 2004.
- [85] D.E. Sheehy and L. Radzihovsky. BEC-BCS crossover in "magnetized" Feshbach-resonantly paired superfluids. *Phys. Rev. Lett.*, 96:060401, 2006.
- [86] J. Kinnunen, L.M. Jensen, and P. Törmä. Strongly interacting Fermi gases with density imbalance. *Phys. Rev. Lett.*, 96:110403, 2006.
- [87] M.M. Parish, F.M. Marchetti, A. Lamacraft, and B.D. Simons. Finite-temperature phase diagram of a polarized Fermi condensate. *Nature Physics*, 3:124, 2007.
- [88] M.M. Parish, S.K. Baur, E.J. Mueller, and D.A. Huse. Quasi-one-dimensional polarized Fermi superfluids. *Phys. Rev. Lett.*, 99:250403, 2007.
- [89] T.K. Koponen, T. Paananen, J.-P. Martikainen, and P. Törmä. Finite temperature phase diagram of a polarized Fermi gas in an optical lattice. *Phys. Rev. Lett.*, 99:120403, 2007.
- [90] E. Zhao and W.V. Liu. Theory of quasi-one-dimensional imbalanced Fermi gases. *Phys. Rev. A*, 78:063605, 2008.
- [91] J. Kinast, S.L. Hemmer, M.E. Gehm, A. Turlapov, and J.E. Thomas. Evidence for superfluidity in a resonantly interacting Fermi gas. *Phys. Rev. Lett.*, 92:15, 2004.
- [92] J. Kinast, A. Turlapov, and J.E. Thomas. Damping of a unitary Fermi gas. *Phys. Rev. Lett.*, 94:17, 2005.
- [93] A. Altmeyer, S. Riedl, C. Kohstall, M.J. Wright, R. Geursen, M. Bartenstein, C. Chin, J. H. Denschlag, and R. Grimm. Precision measurements of collective oscillations in the BEC-BCS crossover. *Phys. Rev. Lett.*, 98:4, 2007.
- [94] L. A. Sidorenkov, M. K. Tey, R. Grimm, Y.-H. Hou, L. Pitaevskii, and S. Stringari. Second sound and the superfluid fraction in a Fermi gas with resonant interactions. *Nature*, 498:78–81, 2013.
- [95] J. Kinast, A. Turlapov, and J. E. Thomas. Breakdown of hydrodynamics in the radial breathing mode of a strongly interacting Fermi gas. *Phys. Rev. A*, 70:051401, 2004.
- [96] A. Altmeyer, S. Riedl, M.J. Wright, C. Kohstall, J.H. Denschlag, and R. Grimm. Dynamics of a strongly interacting Fermi gas: The radial quadrupole mode. *Phys. Rev. A*, 76:3, 2007.
- [97] M. Grasso and M. Urban. Hartree-Fock-Bogoliubov theory versus local-density approximation for superfluid trapped Fermionic atoms. *Phys. Rev. A*, 68:3, 2003.
- [98] G. M. Bruun. Low-energy monopole modes of a trapped atomic Fermi gas. *Phys. Rev. Lett.*, 89:263002, 2002.
- [99] G. M. Bruun and H. Smith. Frequency and damping of the scissors mode of a Fermi gas. *Phys. Rev. A*, 76:045602, 2007.

- [100] R. Cote and A. Griffin. Cooper-pair-condensate fluctuations and plasmons in layered superconductors. *Phys. Rev. B*, 48:10404–10425, 1993.
- [101] A. Korolyuk, J. J. Kinnunen, and P. Törmä. Density response of a trapped Fermi gas: A crossover from the pair vibration mode to the Goldstone mode. *Phys. Rev. A*, 84:033623, 2011.
- [102] P. B. Littlewood and C. M. Varma. Amplitude collective modes in superconductors and their coupling to charge-density waves. *Phys. Rev. B*, 26:4883–4893, 1982.
- [103] G. Vidal. Efficient classical simulation of slightly entangled quantum computations. *Phys. Rev. Lett.*, 91:147902, 2003.
- [104] G. Vidal. Efficient simulation of one-dimensional quantum many-body-systems. *Phys. Rev. Lett.*, 93:040502, 2004.
- [105] S. R. White. Density matrix formulation for quantum renormalization groups. *Phys. Rev. Lett.*, 69:2863–2866, 1992.
- [106] K. Hallberg. New trends in density matrix renormalization. *Advances in Physics*, 55:477–526, 2006.





ISBN 978-952-60-5635-7  
ISBN 978-952-60-5636-4 (pdf)  
ISSN-L 1799-4934  
ISSN 1799-4934  
ISSN 1799-4942 (pdf)

**Aalto University**  
**School of Science**  
**Department of Applied Physics**  
[www.aalto.fi](http://www.aalto.fi)

**BUSINESS +  
ECONOMY**

**ART +  
DESIGN +  
ARCHITECTURE**

**SCIENCE +  
TECHNOLOGY**

**CROSSOVER**

**DOCTORAL  
DISSERTATIONS**